UNCLASSIFIED

SECURITY CLASSIFICATION OF THIS PAGE

DTIC FILE COPY (2)

REPORT DOCUMENTATION PAGE

Form Approved
OMB No 0704-0188
Exp. Date Jun 30, 1986

1a. REPORT SECURITY CLASSIFICATION: UNCLASSIFIED	1b. RESTRICTIVE MARKINGS
2a. SECURITY CLASSIFICATION AUTHORITY	3. DISTRIBUTION/AVAILABILITY OF REPORT: Approved for public release, distribution unlimited
AD-A226 351	5. MONITORING ORGANIZATION REPORT NUMBER(S): AFOSR-TR- 90 0886
6a. NAME OF PERFORMING ORGANIZATION: Arizona State University; 6b. OFFICE SYMBOL (If applicable):	7a. NAME OF MONITORING ORGANIZATION: AFOSR/NA Bolling AFB DC 20332-6448
6c. ADDRESS (City, State, and ZIP Code): Tempe, AZ 85287-6106	7b. ADDRESS (City, State, and ZIP Code): AFOSR/NA Bolling AFB DC 20332-6448
8a. NAME OF FUNDING/SPONSORING ORGANIZATION: AFOSR/NA; 8b. OFFICE SYMBOL (If applicable): AFOSR/NA	9. PROCUREMENT INSTRUMENT IDENTIFICATION NUMBER: AFOSR 87-0237
8c. ADDRESS (City, State, and ZIP Code): AFOSR/NA Bolling AFB DC 20332-6448 Washington, DC 20332-6448	10. SOURCE OF FUNDING NUMBERS: PROGRAM ELEMENT NO. 61102F; PROJECT NO. 2307; TASK NO. A2; WORK UNIT ACCESSION NO

11. TITLE (Include Security Classification)

Navier-Stokes Simulation of Boundary-Layer Transition

12. PERSONAL AUTHOR(S)

Helen L. Reed

13a. TYPE OF REPORT	13b. TIME COVERED	14. DATE OF REPORT (Year, Month, Day)	15. PAGE COUNT
Final	FROM 14 Apr 87 TO 14 Oct 89	May 1990	34

16. SUPPLEMENTARY NOTATION

17. COSATI CODES			18. SUBJECT TERMS (Continue on reverse if necessary and identify by block number)
FIELD	GROUP	SUB-GROUP	laminar boundary layer, Navier-Stokes simulation

19. ABSTRACT (Continue on reverse if necessary and identify by block number)

This Final Report to AFOSR 87-0237, "Navier-Stokes Simulation of Boundary-Layer Transition" describes our successful efforts to computationally model the receptivity of the laminar boundary layer on a semi-infinite flat plate with an elliptic leading edge by a spatial simulation. The incompressible flow is simulated by solving the governing full Navier-Stokes equations in general curvilinear coordinates by a finite-difference method. First, the steady basic-state solution is obtained in a transient approach using spatially varying time steps. Then, small-amplitude acoustic disturbances of the freestream velocity are applied as unsteady boundary conditions, and the governing equations are solved time-accurately to evaluate the spatial and temporal developments of the perturbation leading to instability waves (Tollmien-Schlichting waves) in the boundary layer. The effect of leading-edge radius on receptivity is determined.

The work has been and continues to be closely coordinated with the experimental program

20. DISTRIBUTION/AVAILABILITY OF ABSTRACT	21. ABSTRACT SECURITY CLASSIFICATION
☐ UNCLASSIFIED/UNLIMITED ☒ SAME AS RPT. ☐ DTIC USERS	UNCLASSIFIED
22a. NAME OF RESPONSIBLE INDIVIDUAL: DR JAMES MCMICHAEL	22b. TELEPHONE (Include Area Code): (202) 767-4936
22c. OFFICE SYMBOL: AFOSR/NA	

DD FORM 1473, 84 MAR 83 APR edition may be used until exhausted. All other editions are obsolete.

SECURITY CLASSIFICATION OF THIS PAGE
UNCLASSIFIED

90 08 28 093

19. ABSTRACT

of Professor William Saric, also at Arizona State University, examining the same problems. Comparisons with the experiments at Arizona State University are necessary and an important integral part of this work.

Whenever appropriate, we will match our results from the spatial simulation with triple-deck theory. This is an important aspect of the ongoing work.

FINAL REPORT

for

NAVIER-STOKES SIMULATION OF BOUNDARY-LAYER TRANSITION

AFOSR 87 - 0237

Submitted to

DR. JAMES McMICHAEL

Air Force Office of Scientific Research
Bolling Air Force Base
Washington, D.C. 20332-6448

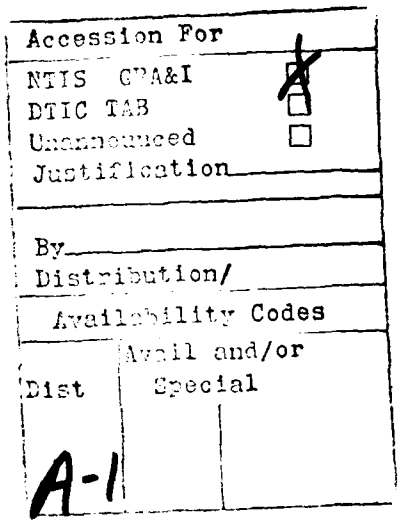

May 1990

Submitted by

HELEN L. REED

Department of Mechanical and Aerospace Engineering
College of Engineering and Applied Science
Arizona State University
Tempe, AZ 85287-6106

John K. Burchard, Ph.D.
Assistant Director,
Office of Research Development & Administration
(602) 965-2170

ABSTRACT

This Final Report to AFOSR 87-0237, "Navier-Stokes Simulation of Boundary-Layer Transition" describes our successful efforts to computationally model the receptivity of the laminar boundary layer on a semi-infinite flat plate with an elliptic leading edge by a spatial simulation. The incompressible flow is simulated by solving the governing full Navier-Stokes equations in general curvilinear coordinates by a finite-difference method. First, the steady basic-state solution is obtained in a transient approach using spatially varying time steps. Then, small-amplitude acoustic disturbances of the freestream velocity are applied as unsteady boundary conditions, and the governing equations are solved time-accurately to evaluate the spatial and temporal developments of the perturbation leading to instability waves (Tollmien-Schlichting waves) in the boundary layer. The effect of leading-edge radius on receptivity is determined.

The work has been and continues to be closely coordinated with the experimental program of Professor William Saric, also at Arizona State University, examining the same problems. Comparisons with the experiments at Arizona State University are necessary and an important integral part of this work.

Whenever appropriate, we will match our results from the spatial simulation with triple-deck theory. This is an important aspect of the ongoing work.

TABLE OF CONTENTS

1. INTRODUCTION

In this Final Report, Section 2 contains a list of related experience and accomplishments from this work. Section 3 presents results from work completed to date. The personnel involved in this project are described in Section 4.

2. RELATED EXPERIENCE AND TECHNICAL ACCOMPLISHMENTS

In the past, 4 students were supervised, 7 publications were written, and 8 talks and lectures were given.

Publications

1. "A Shear--Adaptive Solution of the Spatial Stability of Boundary Layers with Outflow Conditions," H. Haj-Hariri and H.L. Reed, in preparation.

2. "Spatial Simulation of Boundary-Layer Transition," H.L. Reed, *Invited paper*, in preparation for *Appl. Mech. Rev.*

3. "Report of Computational Group," H.L. Reed, in *Transition in Turbines,* NASA CP 2386, NASA Lewis Research Center, May 1984.

4. "Receptivity of the Boundary Layer on a Semi-Infinite Flat Plate with an Elliptic Leading Edge," N. Lin, H.L. Reed, and W.S. Saric, Arizona State University, ASU 90006, Sept. 1989.

5. "Boundary-Layer Receptivity: Computations," N. Lin, H.L. Reed, and W.S. Saric, Third International Congress of Fluid Mechanics, Cairo, Egypt, January 2-4, 1990.

6. "Boundary-Layer Receptivity: Navier-Stokes Computations," H.L. Reed, N. Lin, and W.S. Saric, *Invited Paper*, in *Proceedings of the Eleventh U.S. National Congress of Applied Mechanics*, ASME, New York, 1990.

7. "Navier-Stokes Simulations of Boundary-Layer Receptivity," H.L. Reed, *Keynote Speaker, 22nd Turbulence Symposium*, National Aerospace Laboratory, Tokyo, July 25-27, 1990.

Presentations

1. "Computational Simulation of Transition," H.L. Reed, ICASE Meeting of Stability Theory, NASA/Langley Research Center, Nov. 21, 1986.

2. "Energy-Efficient Aircraft," H.L. Reed, *Invited Talk*, Society of Women Engineers, Notre Dame, Nov. 9, 1988.

3. "A Shear-Adaptive Approach to Spatial Simulations of Transition," H. Haj-Hariri and H.L. Reed, Bull. Amer. Phys. Soc., Vol. 33, No. 10, Nov. 1988.

4. "Boundary-Layer Receptivity: Computations," N. Lin, H.L. Reed, and W.S. Saric,

Bull. Amer. Phys. Soc., Vol. 34, No. 10, Nov. 1989.

Post Doctoral Associates

H. Haj-Hariri, "Spatial Simulation of Transition," completed Spring 1988.

Ph.D. Students

N. Lin, "Boundary-Layer Receptivity to Acoustic Disturbances," expected Spring 1992.

T. Buter, "Boundary-Layer Receptivity to Vortical Disturbances," expected Spring 1992.

C. Lu, "Effect of Initial Conditions on Boundary-Layer Transition," expected Spring 1992.

MS Students

N. Lin, "Receptivity of the Boundary-Layer Flow over a Semi-Infinite Flat Plate with an Elliptic Leading Edge," completed Fall 1989.

The technical accomplishments thus far are documented in the publications listed above. A brief description follows.

"A Shear-Adaptive Solution of the Spatial Stability of Boundary Layers with Outflow Conditions," H. Haj-Hariri and H.L. Reed, in preparation. This work outlines the numerics and boundary conditions used in our spatial simulations of transition.

"Receptivity of the Boundary Layer on a Semi-Infinite Flat Plate with an Elliptic Leading Edge," N. Lin, H.L. Reed, and W.S. Saric, Arizona State University Report CEAS 90006, Sept. 1989. This report demonstrates the feasibility of numerically studying the receptivity problem and establishes the platform upon which our receptivity studies are based. This work represents the first successful numerical treatment of the receptivity problem!

The basic accomplishments that are described in these publications can be outlined as follows:

1. General, three-dimensional spatial stability code developed with curvature to support the experiments and the computations
2. Full Navier Stokes, spatial-simulation numerics developed.
3. Two-dimensional basic-state flow over an elliptic-nosed flat plate established including leading edge and curvature using full Navier Stokes.
4. Freestream disturbance field established for initial/boundary conditions.
5. Two-dimensional disturbance flow over an elliptic-nosed flat plate established including leading edge and curvature using full Navier Stokes.
6. Correlated results of #5 with stability theory of #1.
7. Established platform for receptivity studies for unswept wings.

3. COMPLETED WORK

Boundary-layer receptivity has been discussed in many different forms (Morkovin, 1978, 1983; Mack, 1977; Tani, 1980; to name a few) and has been distinguished by remaining quite opaque. In fact, it is difficult to diagnose whether too little effort has been expended or too little success has been made. However, transition to turbulence will never be successfully understood without answering this fundamental problem (Saric, 1985). The basic question is how freestream turbulence and acoustic signals enter the boundary layer and ultimately generate unstable T-S waves. There is no simple or direct manner for this to happen except in the case of acoustic waves incident on supersonic boundary layers (Mack, 1977). It has long been speculated that the mechanism for freestream disturbances to enter the boundary layer is through the leading-edge region. In this regard, the asymptotic analysis of Goldstein (1983a, 1983b) is encouraging in that it appears to be the first step in analyzing the leading-edge/acoustic-wave problem. The recent experimental work of Leehey and Shapiro (1980) and Gedney (1983) did not focus on the leading edge, and their results have not been completely conclusive. The recent work is summarized by Reshotko (1984) and Goldstein and Hultgren (1989). There is a definite need to continue work in this area with an infusion of new ideas and techniques.

In our work, the receptivity of a flat-plate boundary layer to freestream disturbances was investigated through the numerical solution of the Navier-Stokes equations in the leading-edge region. By stipulating the plate to have finite curvature at the leading edge (a feature left out of some unsuccessful receptivity models), the singularity there was removed and a new length scale introduced. The particular geometry chosen was a semi-ellipse joined to a flat plate. The Reynolds number, based on leading edge curvature, is to be varied parametrically along with the aspect ratio of the ellipse in order to examine the stability of a wide variety of basic states. The use of various aspect ratios covers the range from a sharp leading edge to a semi-circular leading edge to a blunt leading edge.

The main feature of the numerical work here is the use of a body-fitted curvilinear coordinate system to calculate the flow at the elliptic leading-edge region with fine resolution. First, a basic-state solution was obtained by solving the governing equations for steady, incompressible flow with a uniform freestream using a transient approach. Then the basic flow was disturbed by applying time-dependent, forced perturbations as unsteady boundary conditions. The unsteady flow and the temporal and spatial development of the perturbations were determined by numerically solving the unsteady governing equations time accurately. An implicit finite-difference method was used in the streamwise and normal directions and in time. No artificial diffusion was used, yet the numerical methods were found to be robust and stable with the use of reasonably small time steps.

3.1 BASIC-STATE RESULTS

As preliminary results for presentation here, basic-state solutions for steady flow over a semi-infinite flat plate were obtained for two test cases. In calculations, the minor radius of the ellipse was used as a reference length L. The first case corresponds to a rather blunt leading edge with aspect ratio (AR; ratio of major to minor axes) of 3; the second case to a relatively sharp leading edge with aspect ratio 9. See Figures 1 and 2. In both cases, the Reynolds number based on reference length is 2400. The length of the flat plate at the downstream end of the computational box measured from the tip of the ellipse is 45L. The farfield boundary is located at 36L which is 36 times the plate thickness or about 30 times the Blasius boundary-layer thickness at the downstream boundary.

The steady-state flow solutions were obtained in a transient approach with a nondimensional Δt of $0.007 \times AR$ for the first case AR = 3 and a smaller value of Δt of $0.0008 \times$ AR for AR = 9. Altogether, 136 grid points were used in the streamwise direction with approximately 10 grid points in the expected T-S wavelength. In the normal direction 80 grid points were used. In both cases, the grid was stretched such that there were approximately 15 grid points in the boundary layer at the ellipse-flat-plate juncture. The convergence criteria was set as 10^{-8} for maximum residual and absolute error in vorticity and velocity between two time-iteration steps.

Velocity vectors are shown for the two cases in Figures 3 and 4. The velocity vector profiles obtained near the leading edge have some overshoot of the freestream value due to the acceleration over the convex curvature, the overshoot being more pronounced with the blunt leading edge. These profiles verify that solutions obtained by using the boundary-layer assumption or the infinitely sharp flat-plate assumption are missing vital information at the leading edge and are not valid for actual leading edges with finite thickness. The profiles gradually approach profiles with a slight adverse pressure gradient downstream.

Corresponding vorticity profiles at different streamwise locations are shown in Figures 5 and 6. Inflection points are clearly present at the leading-edge region. The pressure gradient along the wall is related to the normal gradient of vorticity at the wall and is shown in Figures 7 and 9. Surface pressure coefficient (C_p) is then obtained by integrating this expression along the wall; this is shown in Figures 8 and 10 along with the corresponding inviscid C_p obtained by a linear surface-panel method. The effect of leading-edge bluntness is illustrated in these figures. The blunt AR = 3 leading edge has a sharp peak (minimum) in surface pressure before recovering rapidly to the freestream pressure and approaching zero pressure gradient. The sharp leading edge has a more rapid approach to the minimum which is smaller (in magnitude) than the minimum in the blunt case. Both surface pressure distributions are close to the inviscid solution except in the rapid pressure-recovery region near the leading edge.

Wall vorticity distributions for the two cases are displayed in Figures 11 and 12. The maximum wall vorticity is 61.9 for the AR = 3 case and occurs at x = 0.12 at the leading edge. For the AR = 9 case, the maximum is 80.5 and occurs at x = 0.09. At the leading edge, the wall vorticity exhibits singularity-like behavior, which is found to be stronger for the AR = 9 case. The blunt case vorticity has a minimum near the leading edge, indicating an approach to separation, but no apparent minimum is observed for the sharp case. Wall vorticity predicted by the boundary-layer assumption underestimates the downstream value.

Another important parameter in presenting the steady flow results is the displacement thickness. Since velocity overshoots occur at the leading edge, the freestream velocity at the boundary-layer edge required in the integration is taken to be the maximum tangential velocity. The nondimensional displacement thickness δ^* should vary as $x^{1/2}$ according to boundary-layer theory. δ^{*2} obtained in the present calculation is plotted as a function of x in Figures 13 and 14 and clearly demonstrates the above linear behavior in the downstream region. δ^* is zero at the stagnation point, remains small in the favorable pressure-gradient region, and rises rather rapidly in the pressure recovery region where the boundary layer thickens. By linear continuation, the location of the virtual leading edge can be approximated. The virtual leading edge occurs at x = -6.0 for AR = 3 and at x = -1.8 for AR = 9; the virtual leading edge approaches the actual one as the leading edge sharpens.

3.2 UNSTEADY-DISTURBANCE RESULTS

Two cases were completed, demonstrating the ability of the present numerical method to perform unsteady time-accurate calculations to simulate receptivity to freestream fluctuations. Both calculations were performed on the AR = 3 flat plate, with the unsteady boundary conditions applied at the farfield being small time-harmonic oscillations of the streamwise velocity with amplitude 10^{-4}, well in the linear range and of the same order of the amplitudes used by Saric in his recent experiments.

In case (1), the oscillations of the freestream streamwise velocity have dimensionless frequency parameter F = 333 ($= 2 \pi \nu f / U_\infty^2 \times 10^6$). Perturbations that eventually develop in the flow will vary at constant forcing frequency, thus following F = constant lines with downstream distance. For F = 333, this line passes above the instability loop according to linear parallel-flow theory (in the stable region), but passes through a narrow unstable region according to some experimental results.

In case (2), the frequency parameter F = 230, which is the value corresponding to the critical point according to linear parallel-flow theory. Branch I of the neutral stability curve

according to linear parallel-flow theory is located at x = 37.9 and the TS wavelength at that point is 4.5. Branch II is at x = 56.2, which is out of the domain considered here.

For F = 333, instantaneous disturbance profiles vs. normal distance from the wall at every streamwise location x are given in Figure 15, after 5 cycles of forcing. After 5 cycles of forcing, when the majority of the flow (except at the region of the convecting disturbance wave front) has become time-periodic (quasi-steady), the amplitude (magnitude) of these periodic perturbations is determined from the last (5th) cycle. The amplitude vs. normal distance from the wall profiles are plotted in Figure 16.

The amplitude of the streamwise perturbation velocity obtained after subtracting the instantaneous Stokes-wave solution, at every streamwise location after x = 3.0 (the juncture of the flat plate and the ellipse) is shown in Figure 17. The amplitude profiles develop into TS wave amplitude profiles around x = 6.0. The receptivity, as defined by the ratio of TS wave amplitude to sound amplitude is of order 1, the maximum being 1.7 at x = 14.05. This trend of order 1 receptivity and the growth of disturbances outside the neutral curve of linear theory was also observed in the experiments (at a higher Reynolds number and lower frequency) by Shapiro (1977) and Leehey and Shapiro (1980). We attribute this to the pressure minimum and the subsequent small adverse pressure gradient near the leading edge. Due to the presence of this small adverse pressure gradient, the instability loop is expected to shift to the left and open up similar to stability diagrams for Falkner-Skan flows.

For F = 230 instantaneous disturbance profiles after 4 periods of forcing, and disturbance amplitude profiles (before the Stokes wave is subtracted) with respect to normal distance during the fourth cycle are given in Figures 18 and 19. After the Stokes wave is subtracted, disturbance profiles displayed in Figure 20 show clearly a transformation into TS wave profiles. The wavelength is 4.5 and the wavespeed is 0.395, which are about the same as the TS wavelength and wavespeed according to linear stability theory. The ratio of maximum amplitude of the TS wave to the sound-wave amplitude is about 0.8, the maximum occurring at three grid points between x = 20.58 and x = 21.39. Compared to the high-frequency case (1), the amplitudes of the TS wave in this case are found to be smaller. We attribute this to the fact that the Branch I neutral point for a lower value of F is farther downstream (according to linear stability theory).

3.3 CONCLUSIONS FROM COMPLETED WORK

A numerical code has been developed to solve both steady and unsteady two-dimensional flow over a flat plate with an elliptic leading edge and finite thickness using the full incompressible Navier-Stokes equations in curvilinear coordinates. The present time-accurate code has allowed us to observe both the temporal and spatial initial development of the instability (TS) wave in the boundary layer due to imposed, freestream, long-wavelength

disturbances. This is the first successful attempt to numerically simulate receptivity to freestream, time-harmonic oscillations on a realistic flat plate, offering possible explanations for discrepancies between experiments and various simplified numerical and theoretical models.

Some of the important conclusions that can be inferred thus far are:

i) The experimental results of early growth of TS waves before the Branch I neutral-stability point and order 1 receptivity are observed, and can be attributed to the adverse pressure gradient existing near the blunt leading edge.

ii) The observance of TS wave growth with F = 333 is in accordance with some experimental observations and indicates that the discrepancies in neutral stability curves between linear stability theory and experiments at high frequencies can be due to small mean adverse pressure gradients existing near the leading edge.

iii) The receptivity mechanism to freestream, time-harmonic, long-wavelength oscillations, which has been observed in experiments is verified to some extent in this study and can be described as follows:

A long-wavelength, streamwise velocity perturbation, which closely simulates a plane sound wave travelling parallel to the plate in an incompressible limit, has to diffract at the leading edge, which introduces spatial variations in fluctuations of both u' and v' components at the leading edge (near the stagnation point), or, in other words, introduces unsteady fluctuations in pressure that vary with tangential direction along the wall. This, in turn, generates fluctuating vorticity at the leading edge, the majority of which is convected downstream in the boundary layer. This convected vorticity wave soon matches or develops into instability waves (TS waves) of the laminar boundary layer.

iv) Up to the periods of calculations presented here, interaction between the TS wave and the travelling sound wave occurs only at the leading edge region.

v) Some qualitative features predicted by the theory of Goldstein (1983) are observed, although the orders of receptivity differ. The quantitative measure of receptivity here, i.e. the ratio of amplitude of the TS wave to that of the freestream disturbance, definitely depends on the leading-edge radius of curvature, and hence the pressure gradient there.

4. RESOURCES AND PERSONNEL

The principal investigator for this work was Helen L. Reed, Associate Professor of Mechanical and Aerospace Engineering. Professor Reed has spent the last nine years conducting theoretical and computational research on problems of boundary-layer stability specifically applied to the ACEE/LFC programs.

Nay Lin was the principle graduate student supported by this grant. He very successfully

completed his MS thesis "Receptivity of the Boundary Layer on a Semi-Infinite Flat Plate with an Elliptic Leading Edge," in the Fall of 1989.

Professor William S. Saric participated as a consultant to the program. He brought with him fifteen years of experience conducting theoretical and experimental research on problems of boundary-layer stability and transition. His research is closely coordinated with the computational work.

One of the principal strengths of our team at Arizona State University is its broad skills in analysis, computations, and experiments. We facilitate day-to-day communication between the computational work and the experimental work through an IRIS 3030 Graphics Workstation. The system, with state-of-the-art, real-time, three-dimensional, color-graphics software (PLOT3D), is equipped with an extensive multi-user and multi-task environment with twelve serial lines. Users are able to share the same data base or experimental information. This provides the heart of the interaction of the analytical, computational, and experimental research.

In addition to the super computers at AFOSR facilities and Princeton/NSF Consortium, the network includes access to the IBM 4341/VM and Harris/VS computers, the IBM 3090 Class VI machine, and the Cray on campus as well as the MASSCOMP. The College of Engineering at ASU is currently also equipped with several VAX/780 and VAX/785 minicomputers exclusively for research purposes (each office and laboratory has a hard-wired RS232 interface). These minicomputers are excellent systems for program development. The IRIS can access all the features available in those minicomputers through the existing local area networking (Ethernet) on the campus. Furthermore, the system can communicate directly with AFOSR research facilities to share information through telephone couplings. The full array of computer capabilities from super-mini to super-super was in place for the research.

5. REFERENCES

Gedney, C.J. 1983. The cancellation of a sound-excited Tollmien-Schlichting wave with plate vibration. Phys. Fluids 26, 5, 1158-1160.

Goldstein, M.E. 1983a. The evolution of Tollmien-Schlichting waves near a leading edge. J. Fluid Mech. 127. 59.

Goldstein, M.E., Sockol, P.M. and Sanz, J. 1983b. The evolution of Tollmien-Schlichting waves near a leading edge. Part 2. Numerical determination of amplitudes. J. Fluid Mech. 129, 443.

Goldstein, M.E. and Hultgren, L.S. 1989. Boundary-layer receptivity to long-wave free-stream disturbances. Ann. Rev. Fluid Mech. 21, 137-66.

Leehey, P. and Shapiro, P.J. 1980. Leading edge effect in laminar boundary layer excitation by sound. Laminar-Turbulent Transition, Springer-Verlag, 321-331.

Mack, L.M. 1977. Transition prediction and linear stability theory. AGARD C-P No. 224, 1.

Morkovin, M.V. 1978. Instability, transition to turbulence and predictability. AGARDograph No. 236.

Morkovin, M.V. 1983. Understanding transition to turbulence in shear layers - 1983. AFOSR Final Report, Contract F49620-77-C-0013.

Reshotko, E. 1984. Environment and receptivity. AGARD Report No. 709 (Special course on stability and transition of laminar flows) VKI, Brussels, March 1984.

Saric, W.S. 1985a. Stability and transition in bounded shear flows. Proc. Persp. Fluid Mech., Caltech, Jan. 1985.

Saric, W.S. 1985b. Boundary-layer transition: T-S waves and crossflow mechanisms. Proc. AGARD Special Course on Aircraft Drag Prediction and Reduction, VKI, Belgium, May 1985.

Saric, W.S. 1985c. Laminar flow control with suction: theory and experiment. Proc. AGARD Special Course on Aircraft Drag Prediction and Reduction, VKI, Belgium, May 1985.

Shapiro, P.J. 1977. The influence of sound upon laminar boundary layer instability. MIT Acoustics & Vibration Lab. rep. 83458-83560-1.

Singer, B.A., Reed, H.L. and Ferziger, J.H. 1989. The effect of streamwise vortices on transition in the plane channel. Accepted Phys. Fluids.

Tani, I. 1980. Three-dimensional aspects of boundary-layer transition. Reprint: Visiting Scholar Lectures, VPI & SU, Oct. 1980.

6. FIGURES

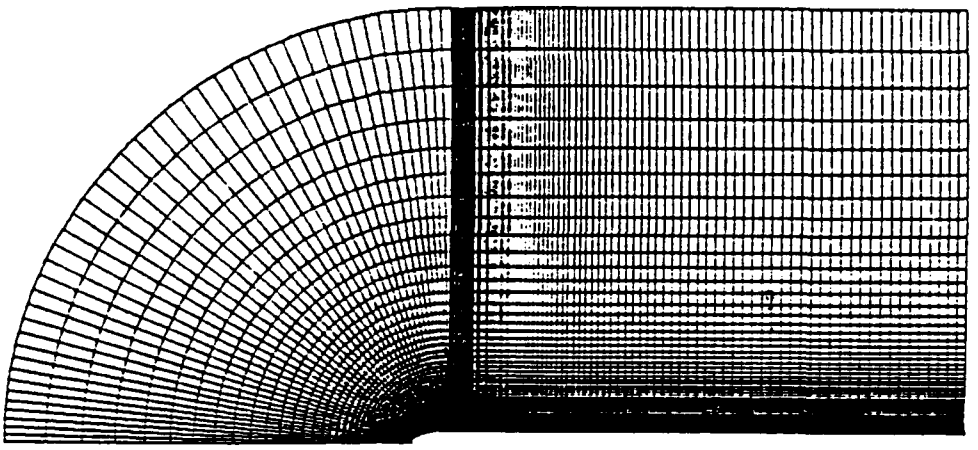

a. Generated C-grid

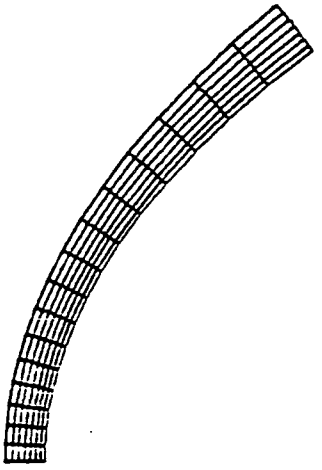

b. Enlarged view at the leading edge

Figure 1. Generated grid over the semi-infinite flat plate; AR=3.

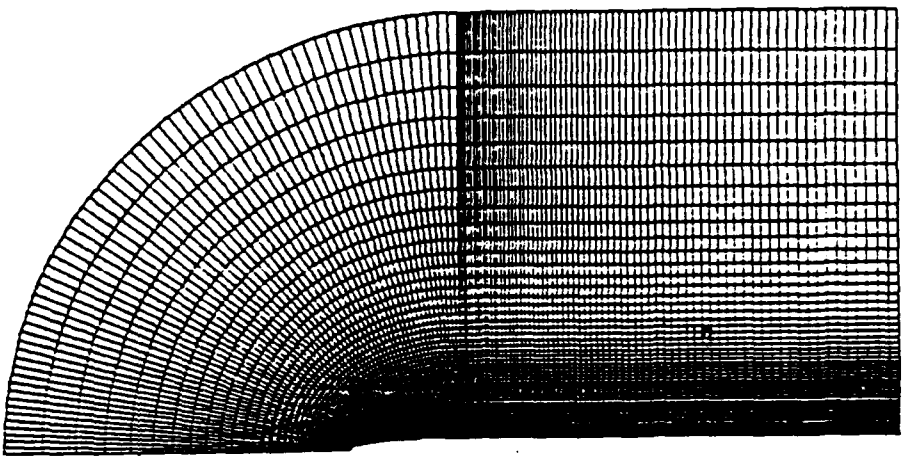

a. Generated C-grid

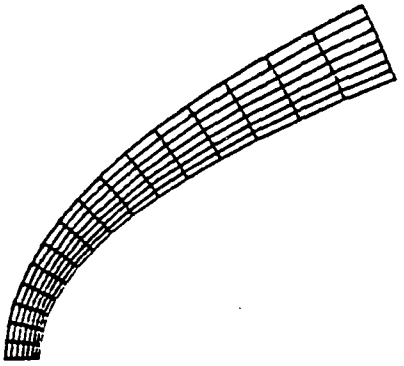

b. Enlarged view at the leading edge

Figure 2. Generated grid over the semi-infinite flat plate; AR=9.

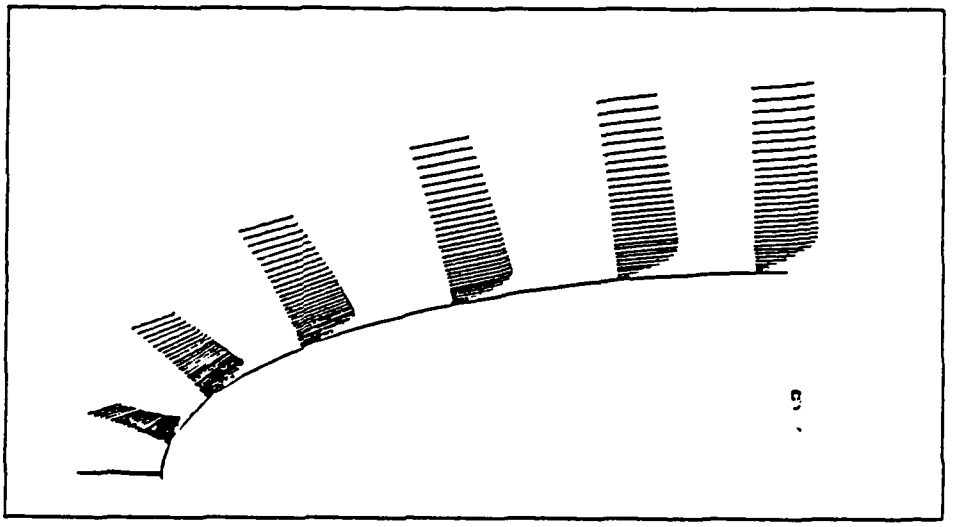

a. Leading edge region.

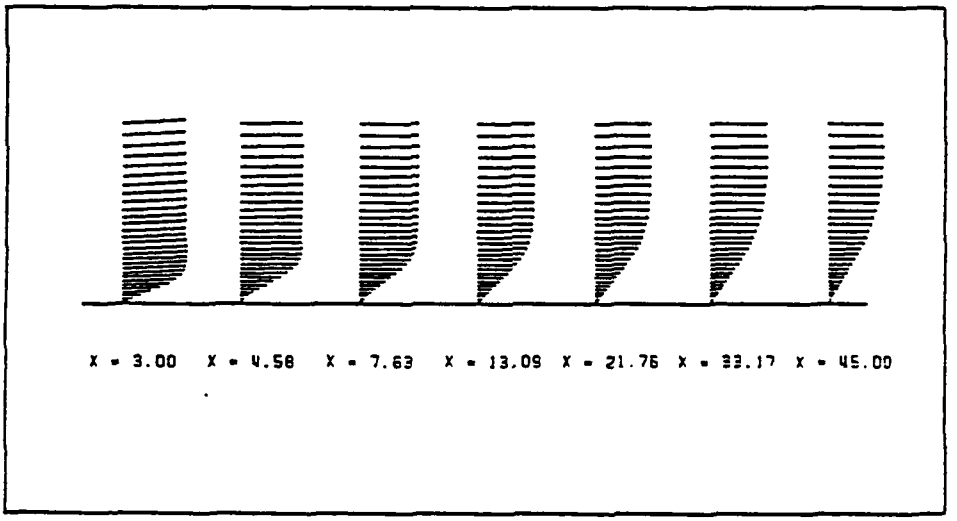

b. Flat plate region.

Figure 3. Steady state velocity vector profiles ; AR = 3, Re_L = 2400.

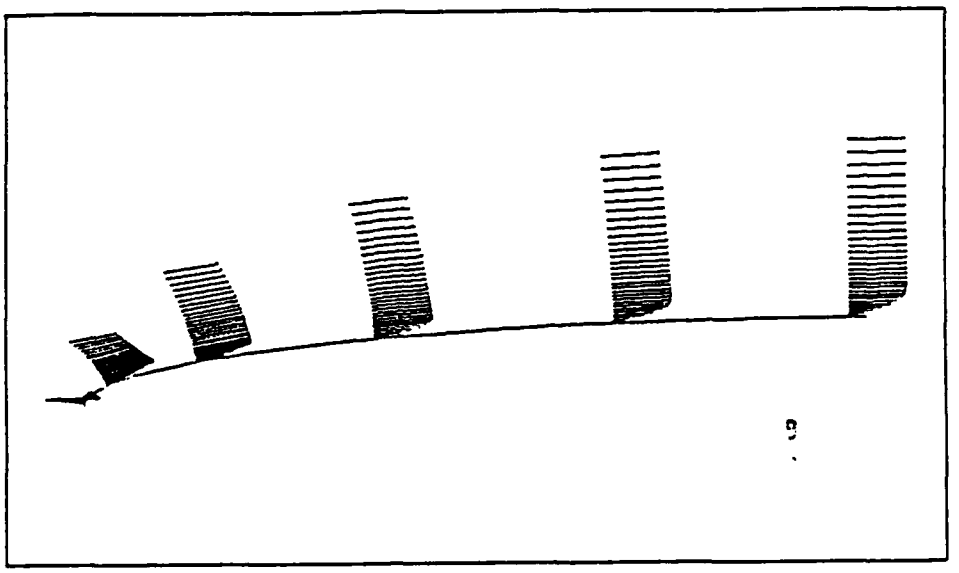

a. Leading edge region.

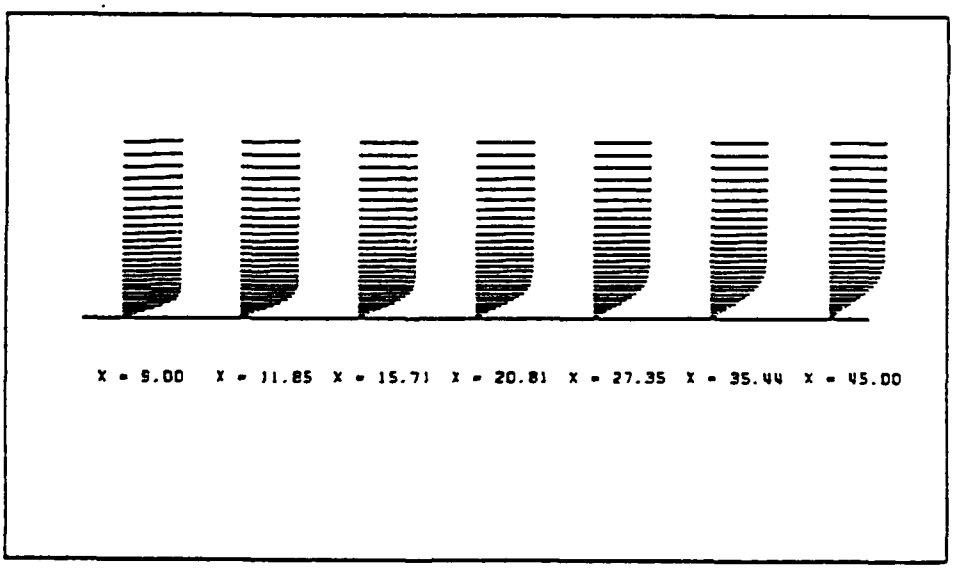

b. Flat plate region.

Figure 4. Steady state velocity vector profiles ; AR = 9, Re_L = 2400.

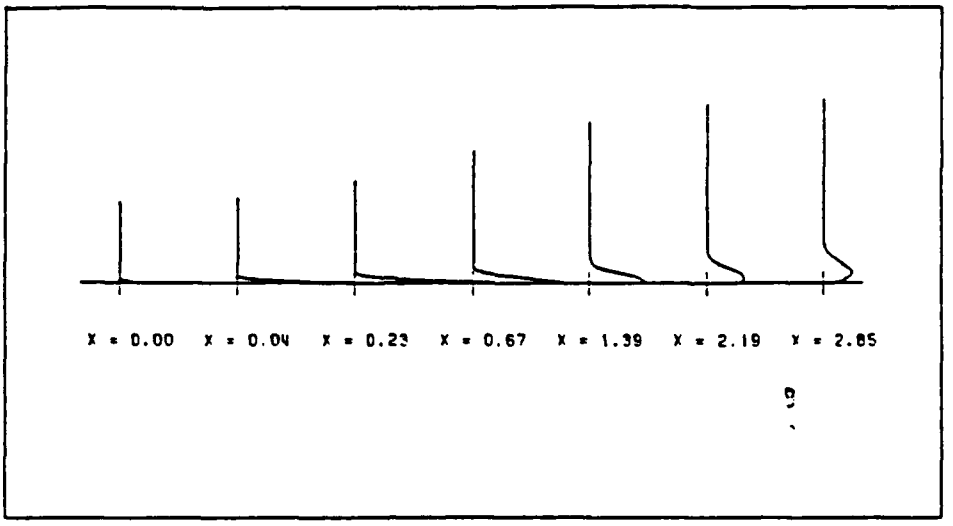

a. Leading edge region.

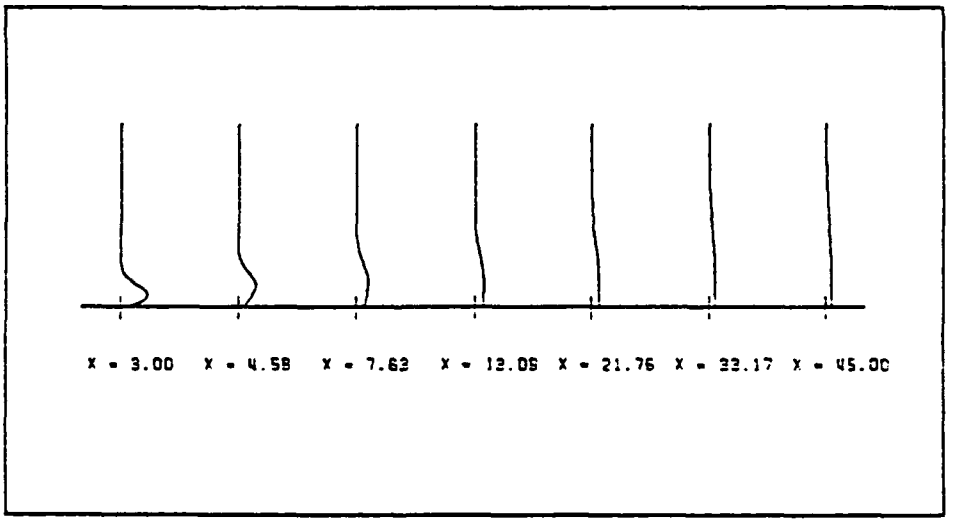

b. Flat plate region.

Figure 5. Steady state vorticity profiles vs. normal distance; AR = 3, Re_L = 2400.

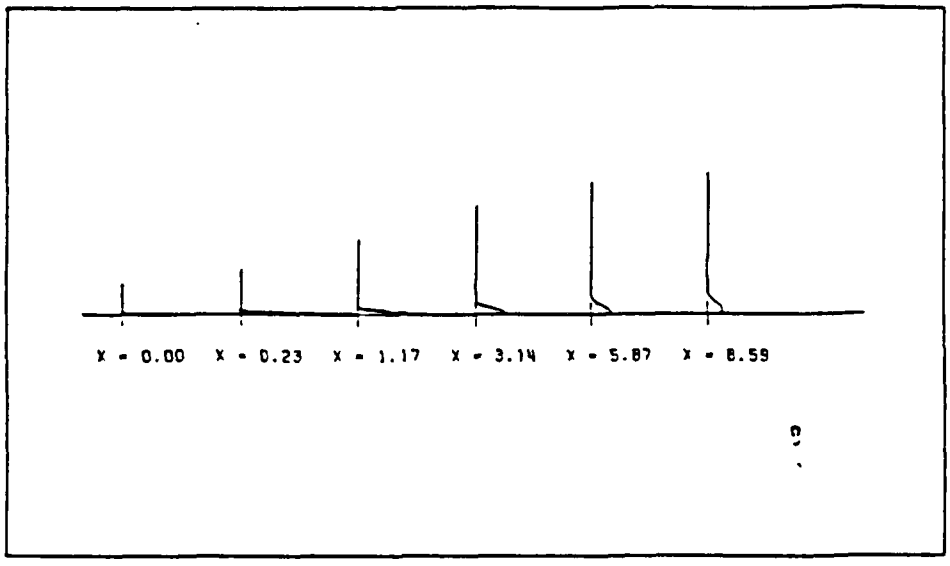

a. Leading edge region.

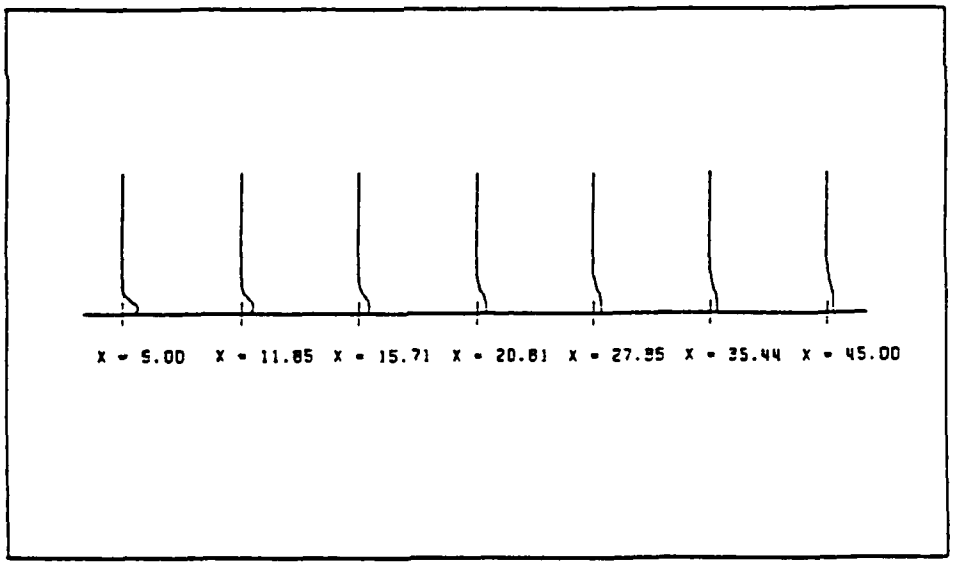

b. Flat plate region.

Figure 6. Steady state vorticity profiles vs. normal distance; AR = 9, Re_L = 2400.

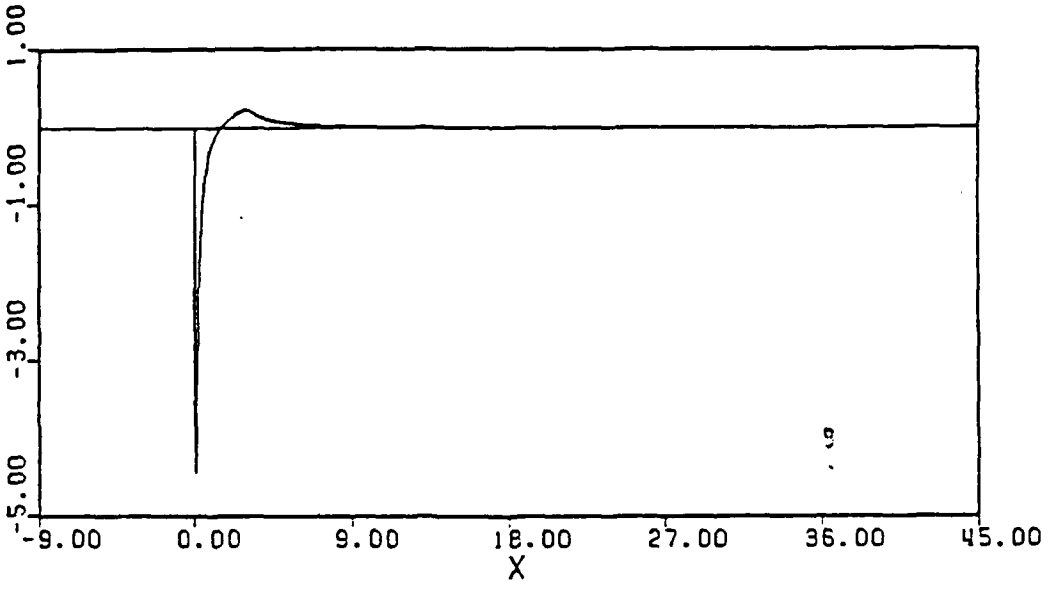

Figure 7. Pressure gradient along the wall; AR = 3, Re_L = 2400.

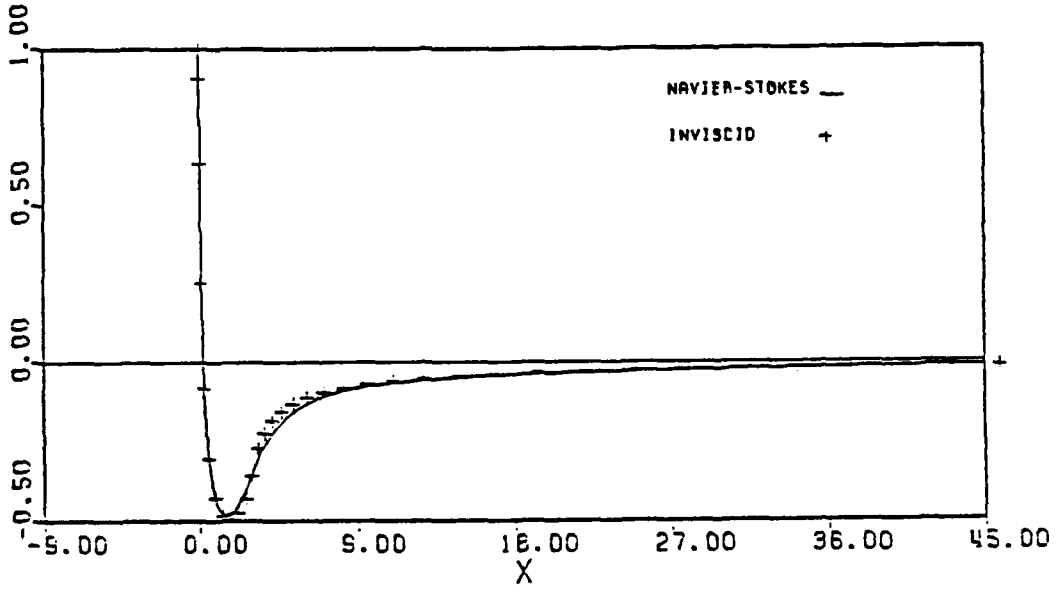

Figure 8. Surface pressure coefficient C_p; AR = 3, Re_L = 2400.

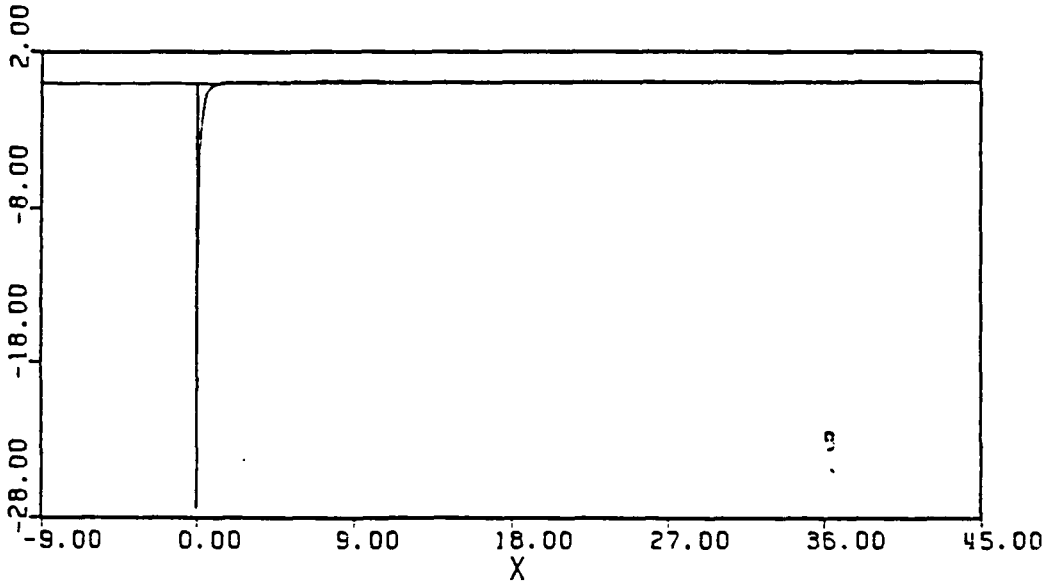

Figure 9. Pressure gradient along the wall; AR = 9, Re_L = 2400.

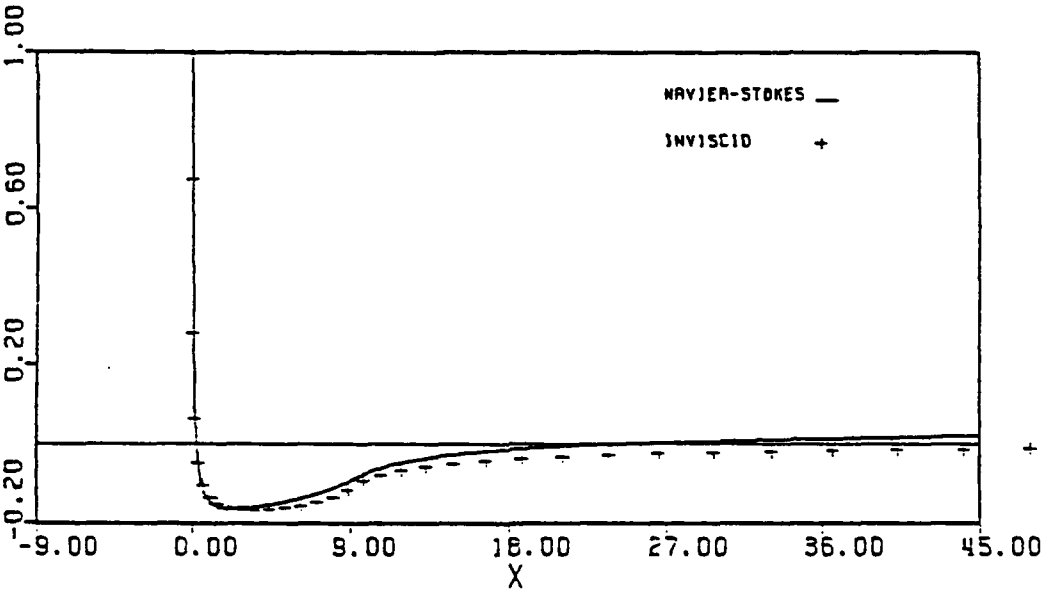

Figure 10. Surface pressure coefficient C_p; AR = 9, Re_L = 2400.

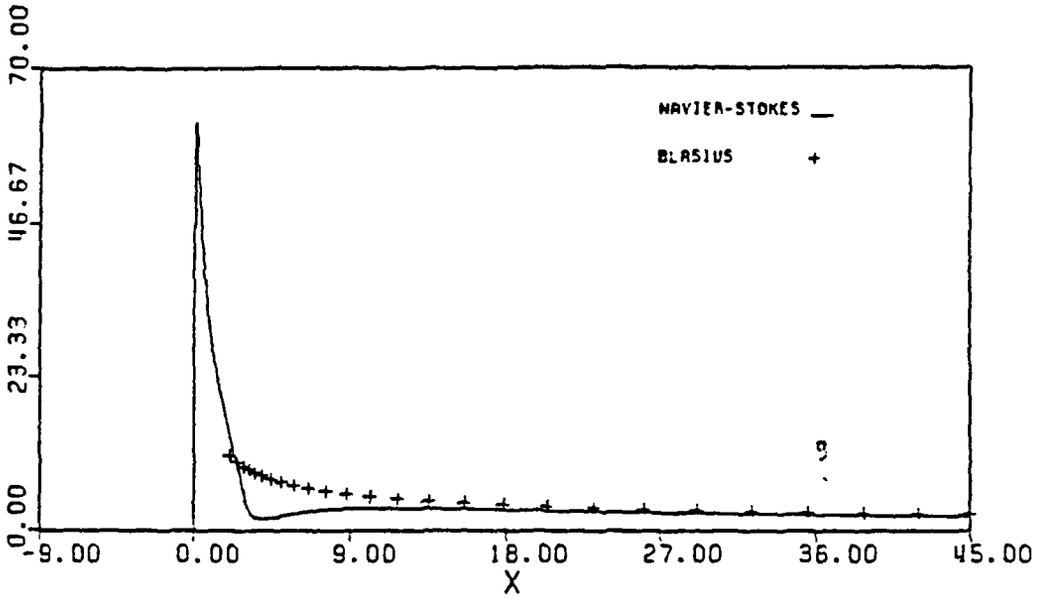

Figure 11. Wall vorticity distribution; AR = 3, Re_L = 2400.

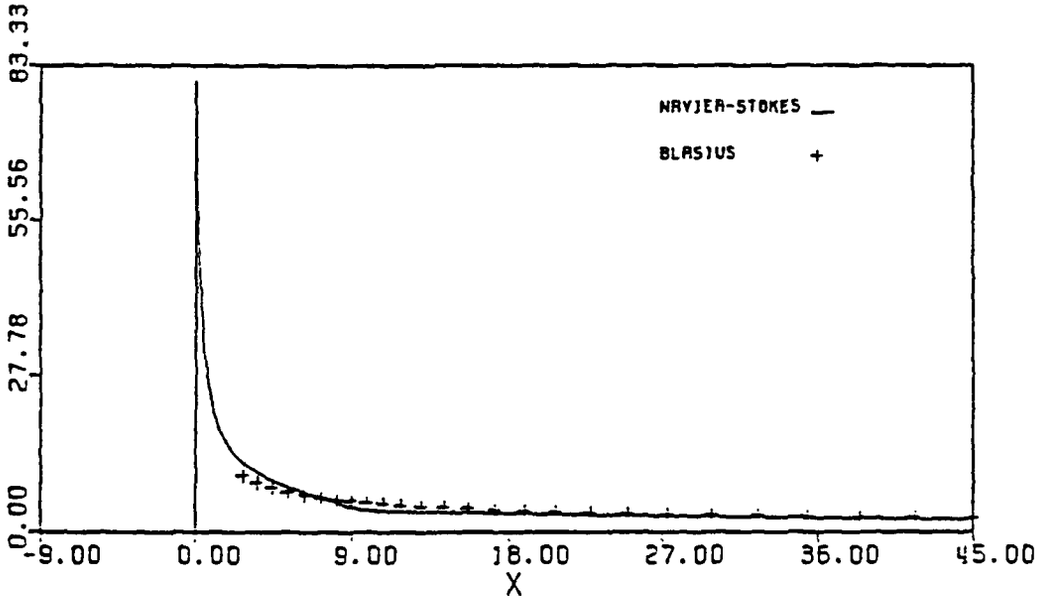

Figure 12. Wall vorticity distribution; AR = 9, Re_L = 2400.

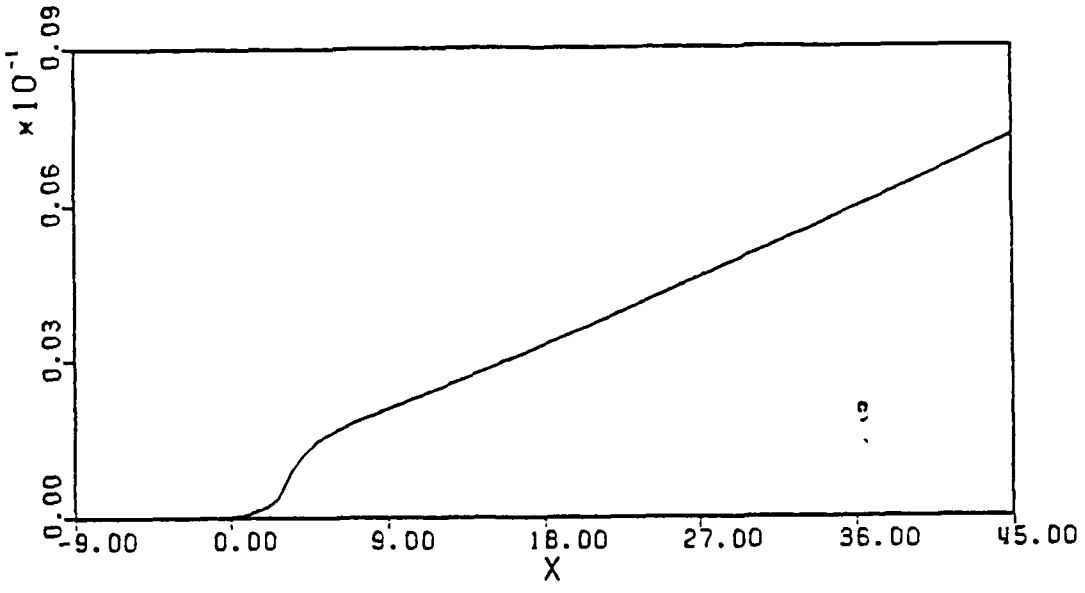

Figure 13. Square of the displacement thickness δ^{*2} vs. x; AR=3, Re_L = 2400.

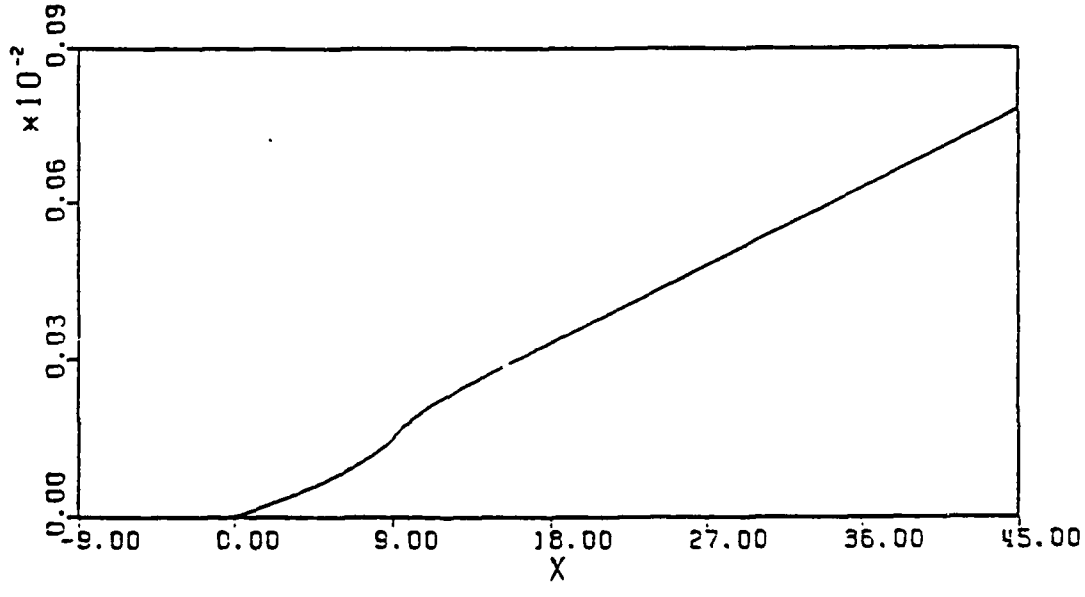

Figure 14. Square of the displacement thickness δ^{*2} vs. x; AR = 9, Re_L = 2400.

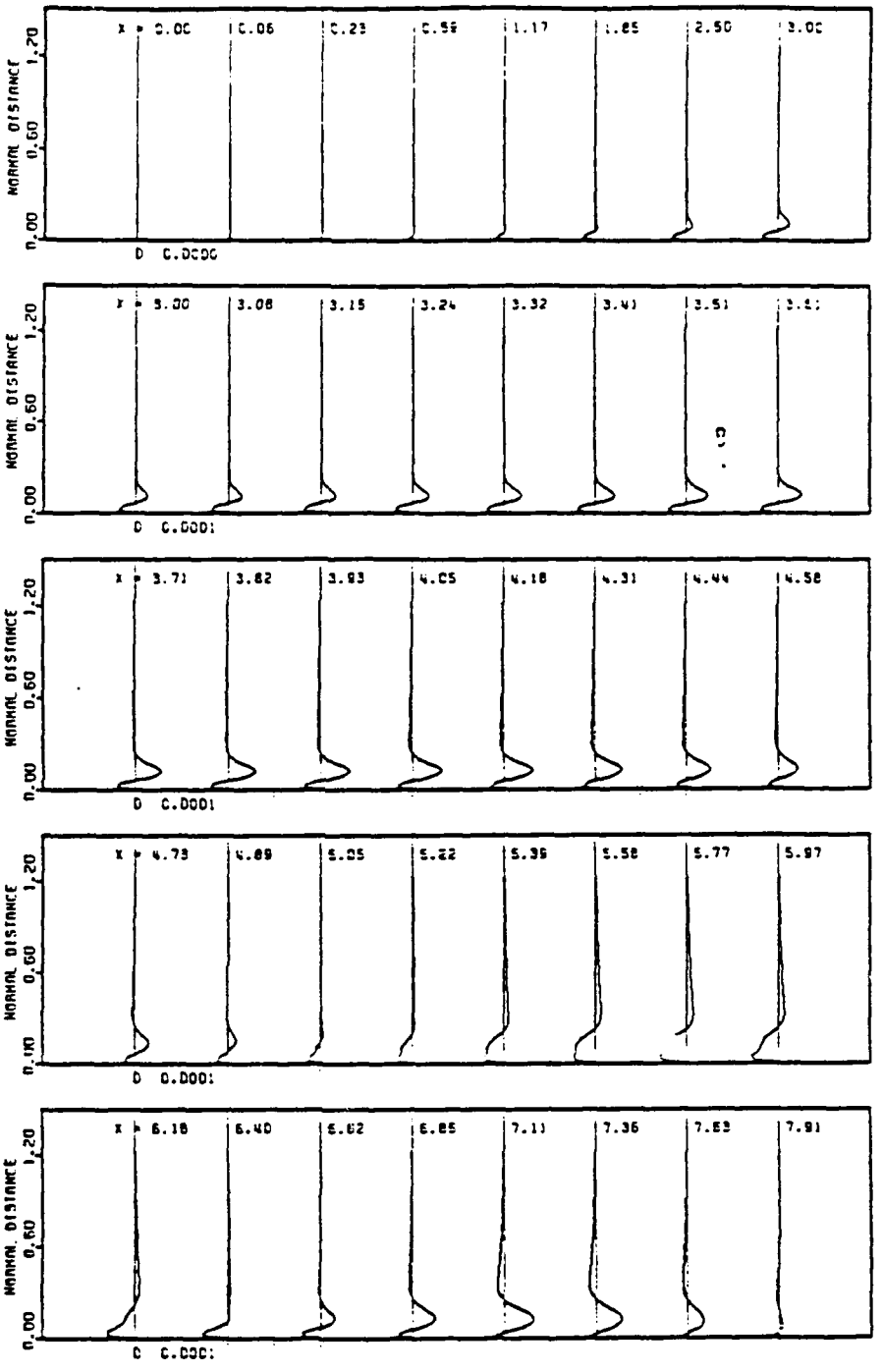

a. streamwise perturbation velocity, u'

Figure 15. Instantaneous perturbation profiles at consecutive downstream locations after five periods of forcing ; F = 325, a_s= 0.0001.

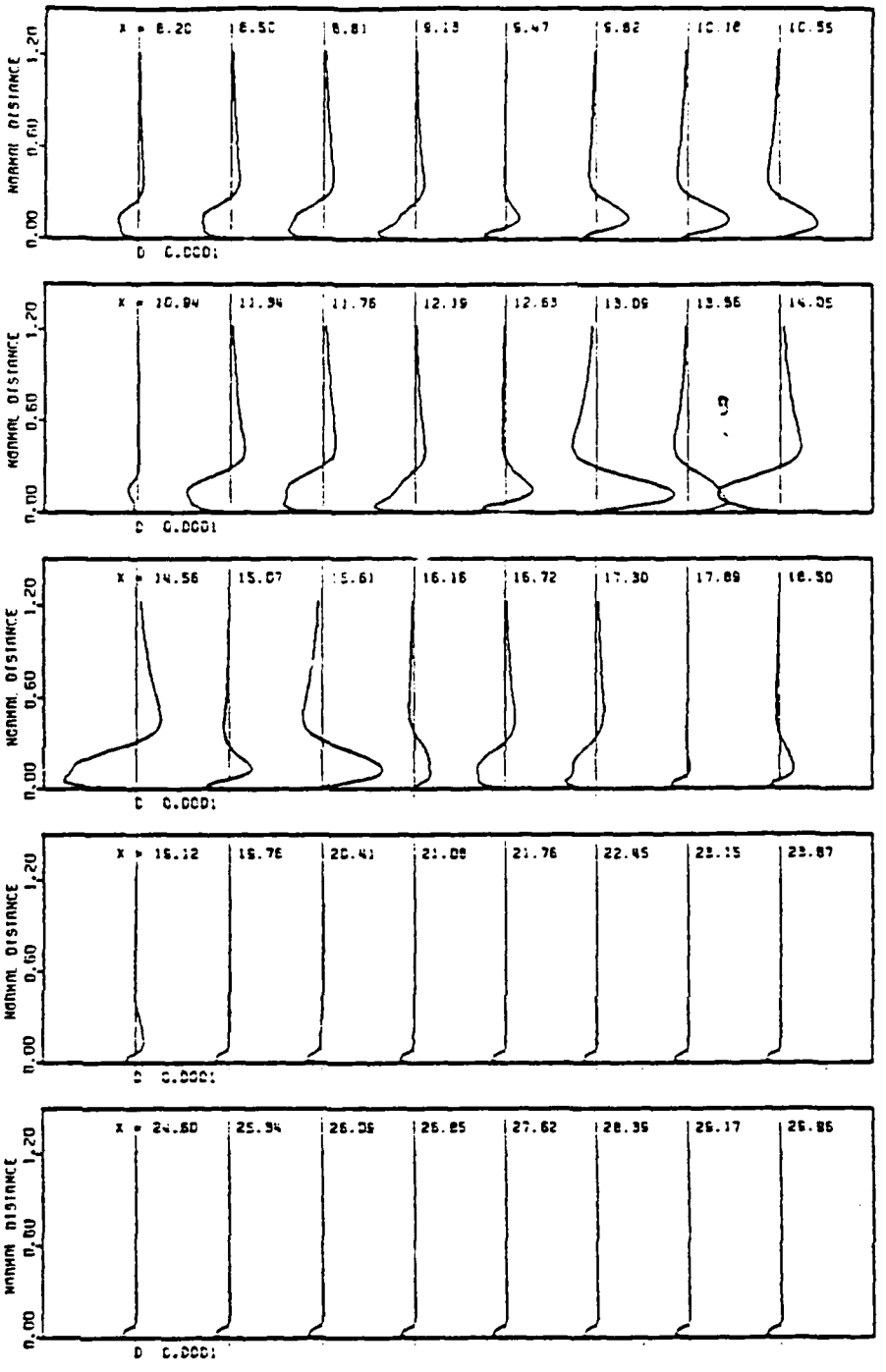

Figure 15a. Continued.

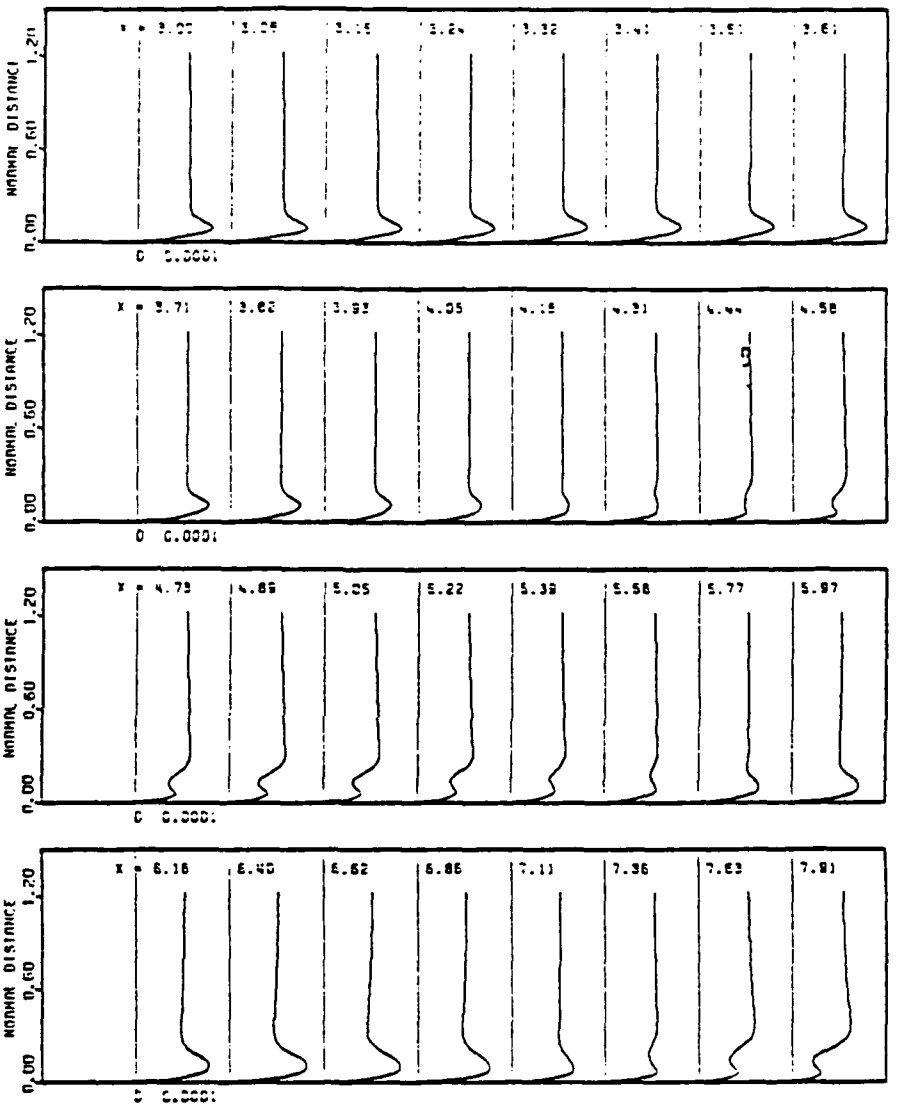

a. streamwise perturbation velocity, u'

Figure 16. Perturbation amplitude profiles taken during the fifth cycle at consecutive downstream locations before the Stokes wave is subtracted; F = 325, a_S= 0.0001.

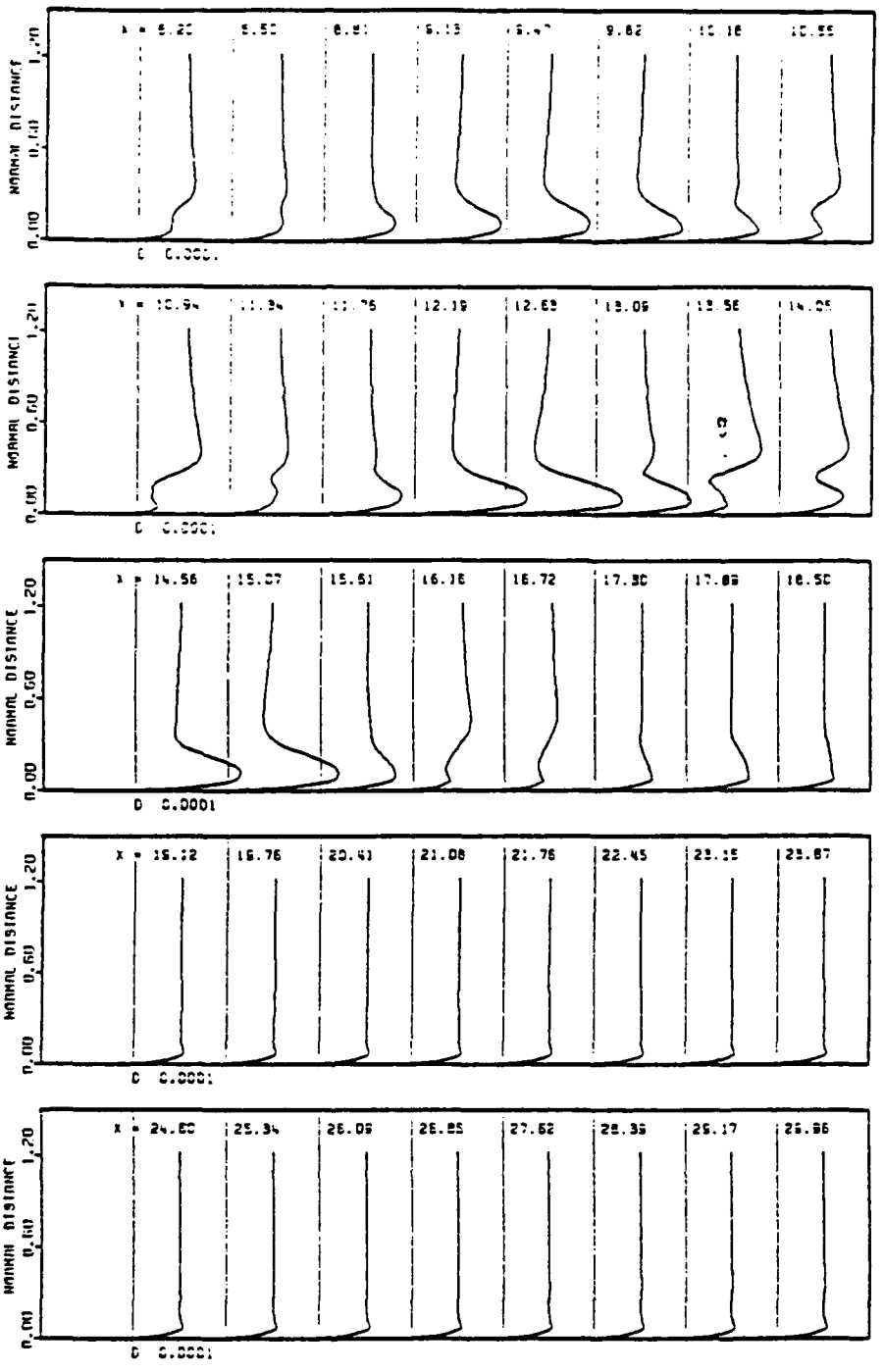

Figure 16a. Continued.

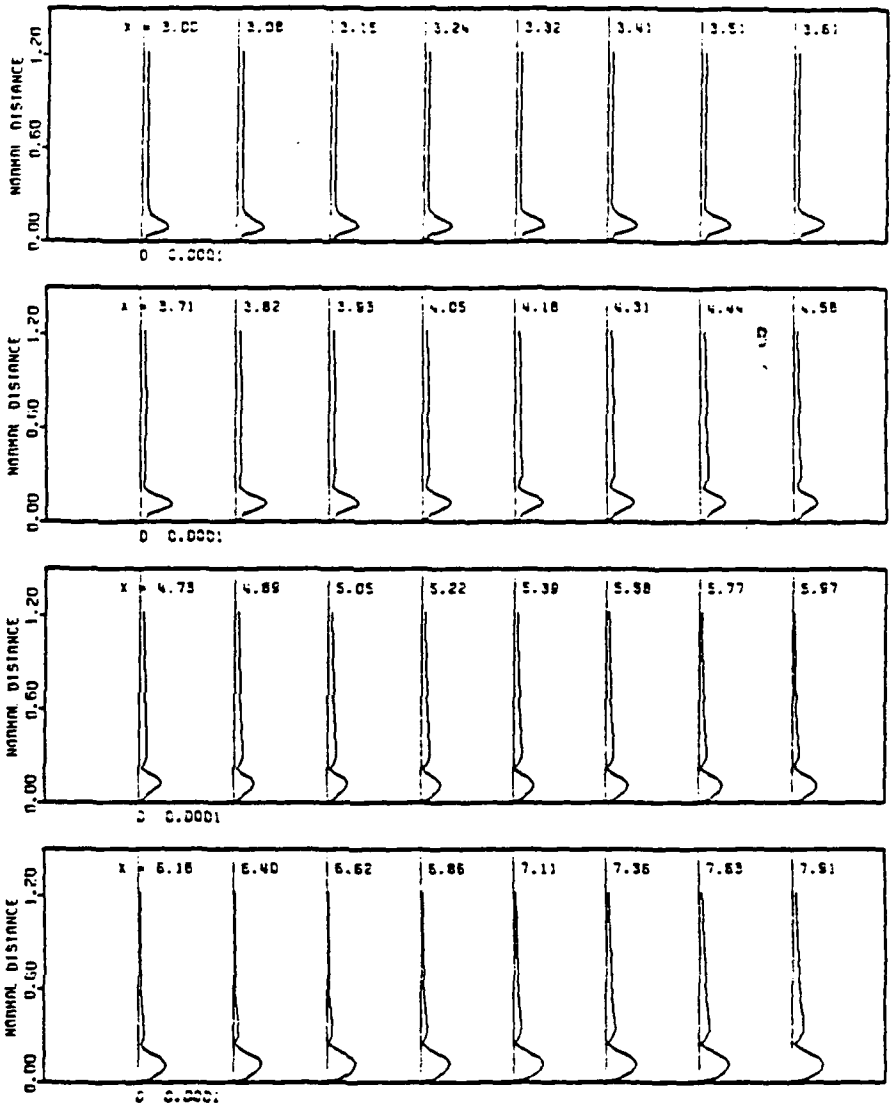

Figure 17. Amplitude profiles of streamwise perturbation velocity u' taken during the fifth cycle at consecutive downstream locations after the Stokes wave is subtracted; F = 325, a_s= 0.0001.

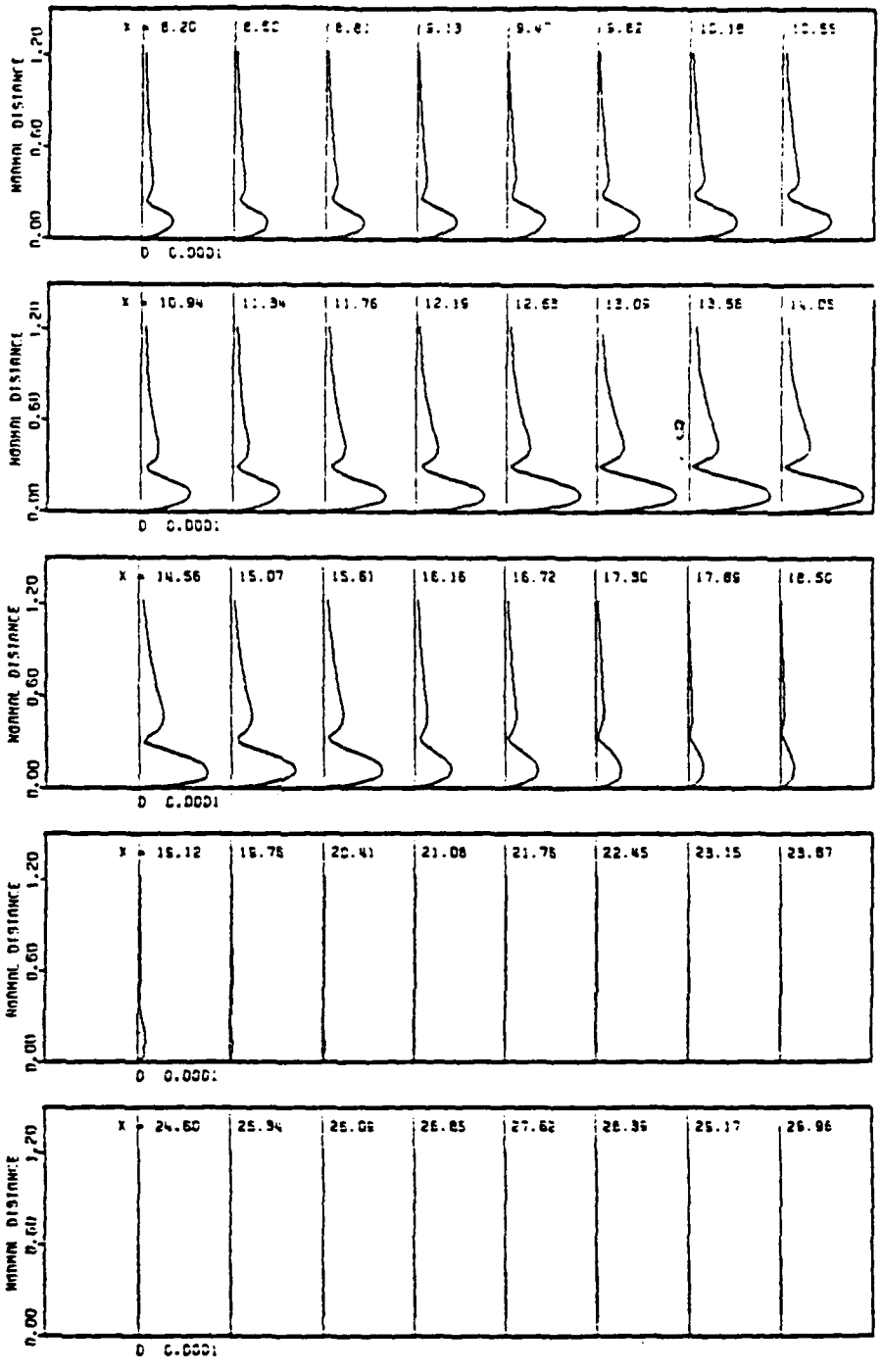

Figure 17a. Continued.

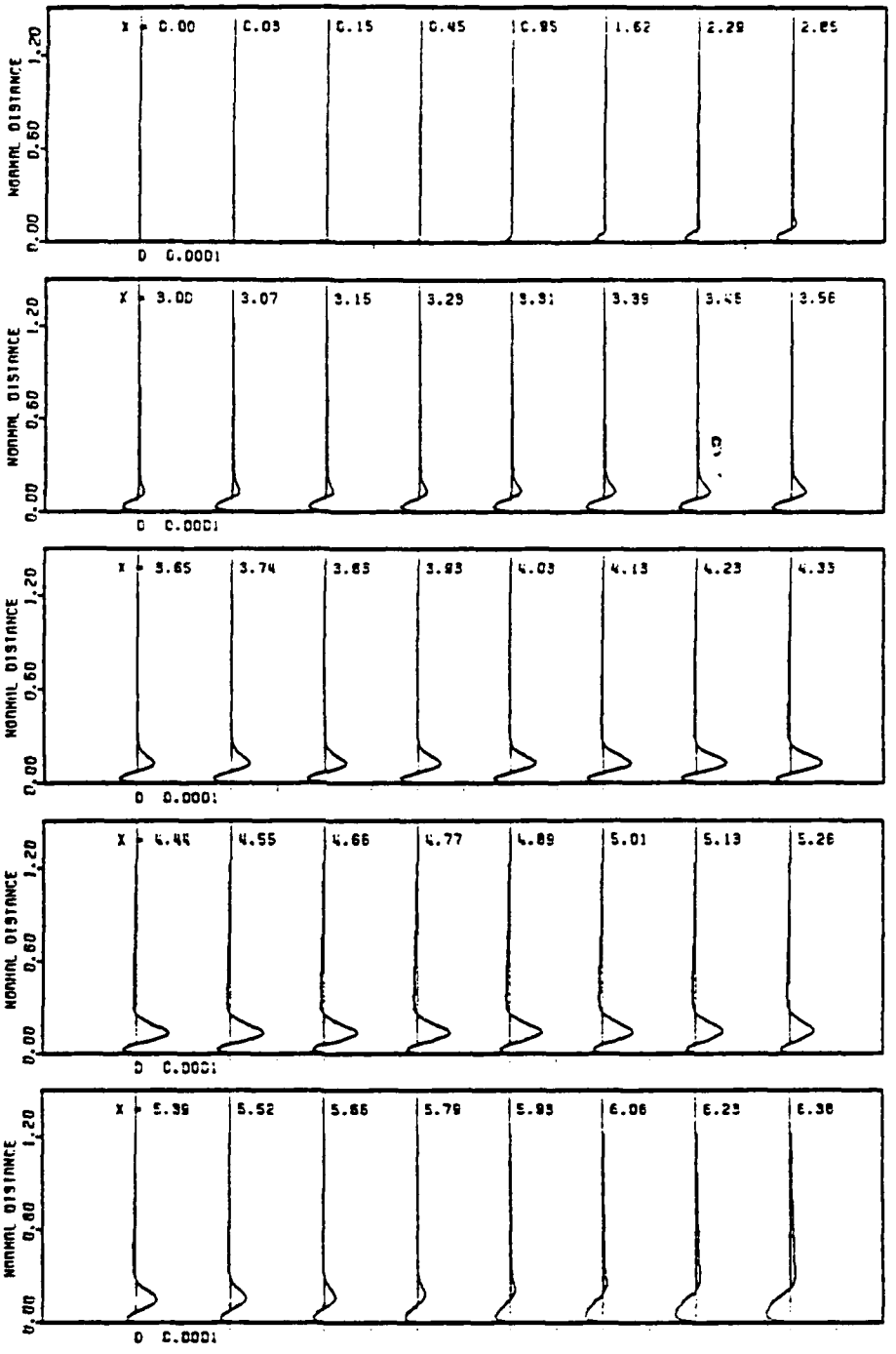

a. streamwise perturbation velocity, u'

Figure 18. Instantaneous perturbaton profiles at consecutive downstream locations after four periods of forcing; F = 230, a_S= 0.0001.

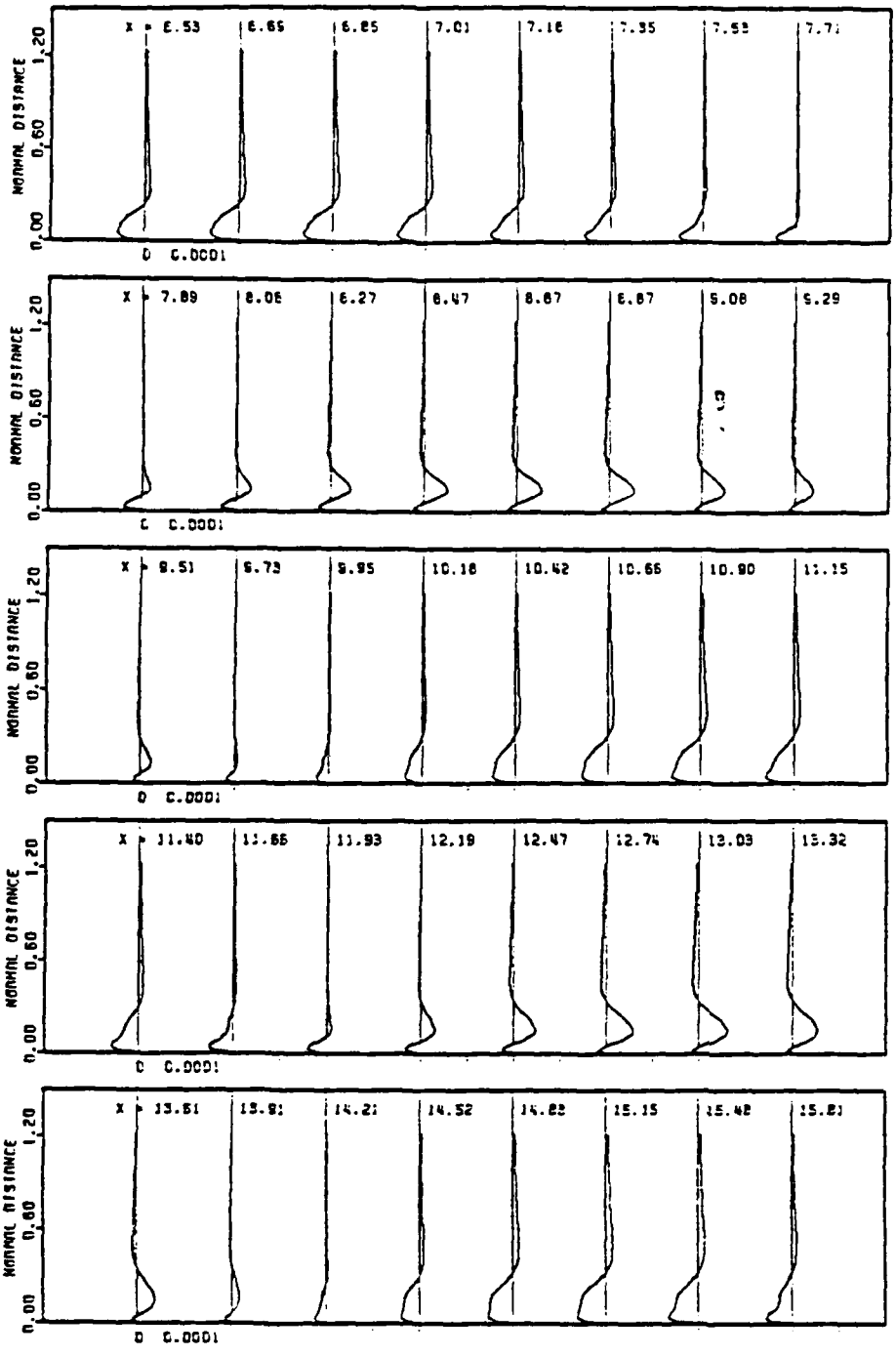

Figure 18a. Continued.

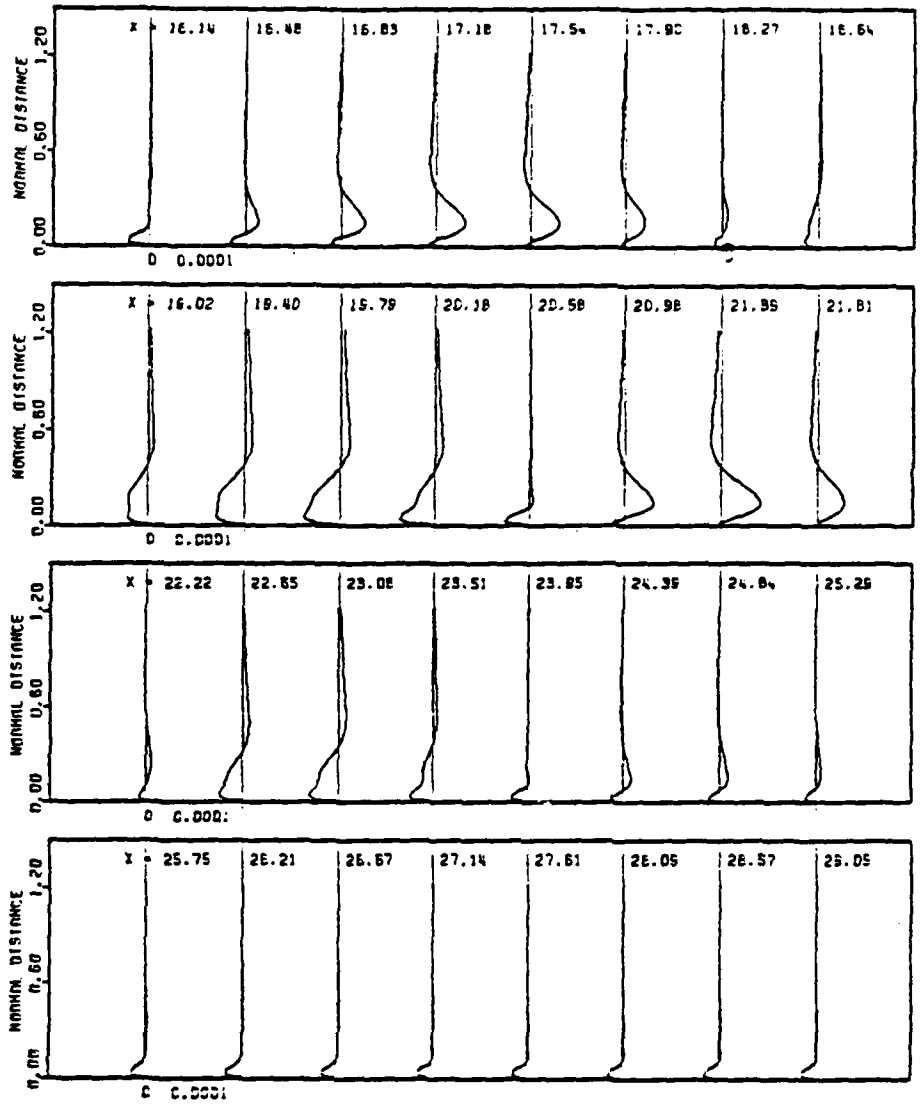

Figure 18a. Continued.

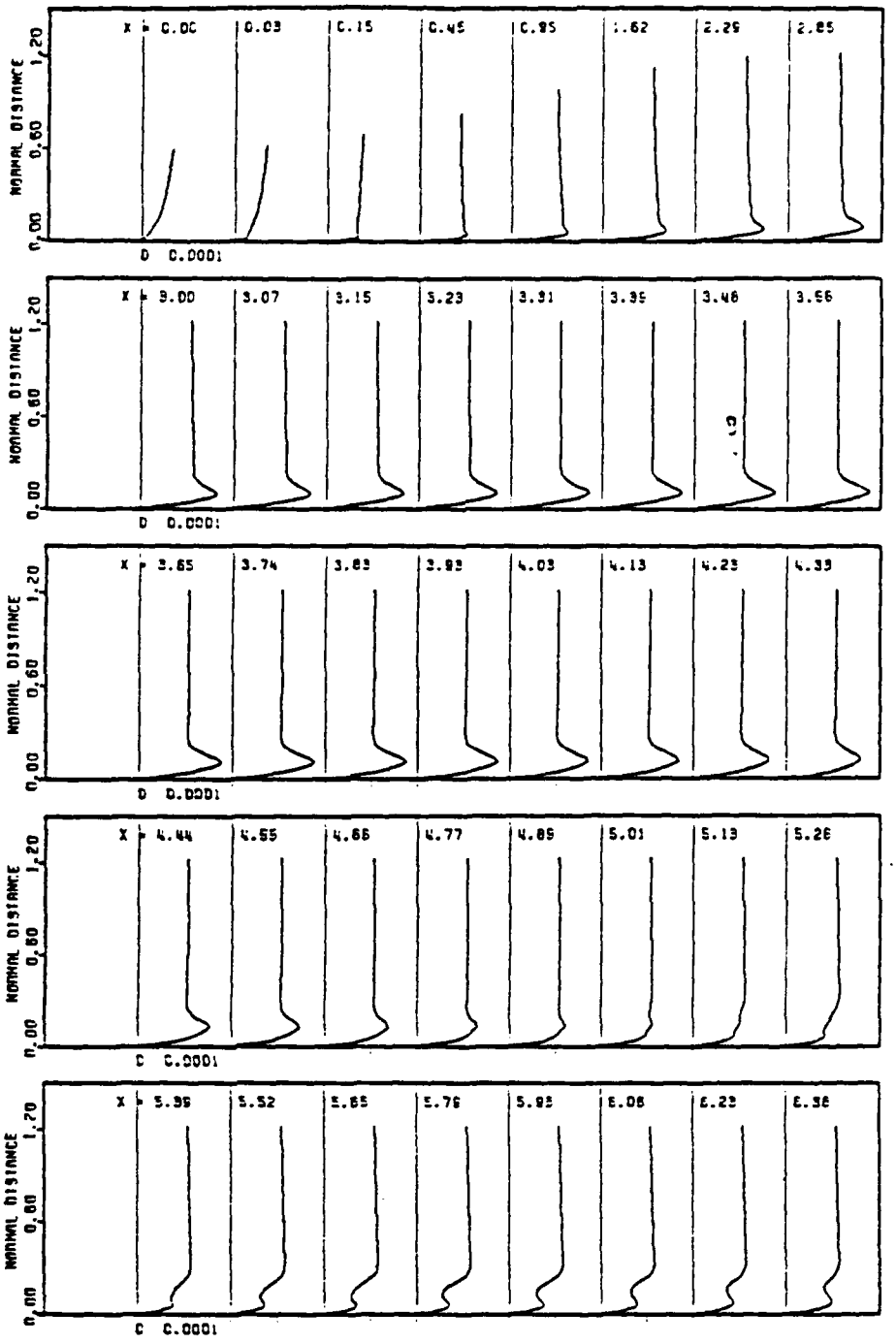

a. streamwise perturbation velocity, u'

Figure 19. Perturbation amplitude profiles taken during the fourth cycle at consecutive downstream locations before the Stokes wave is subtracted; F = 230, a_S= 0.0001.

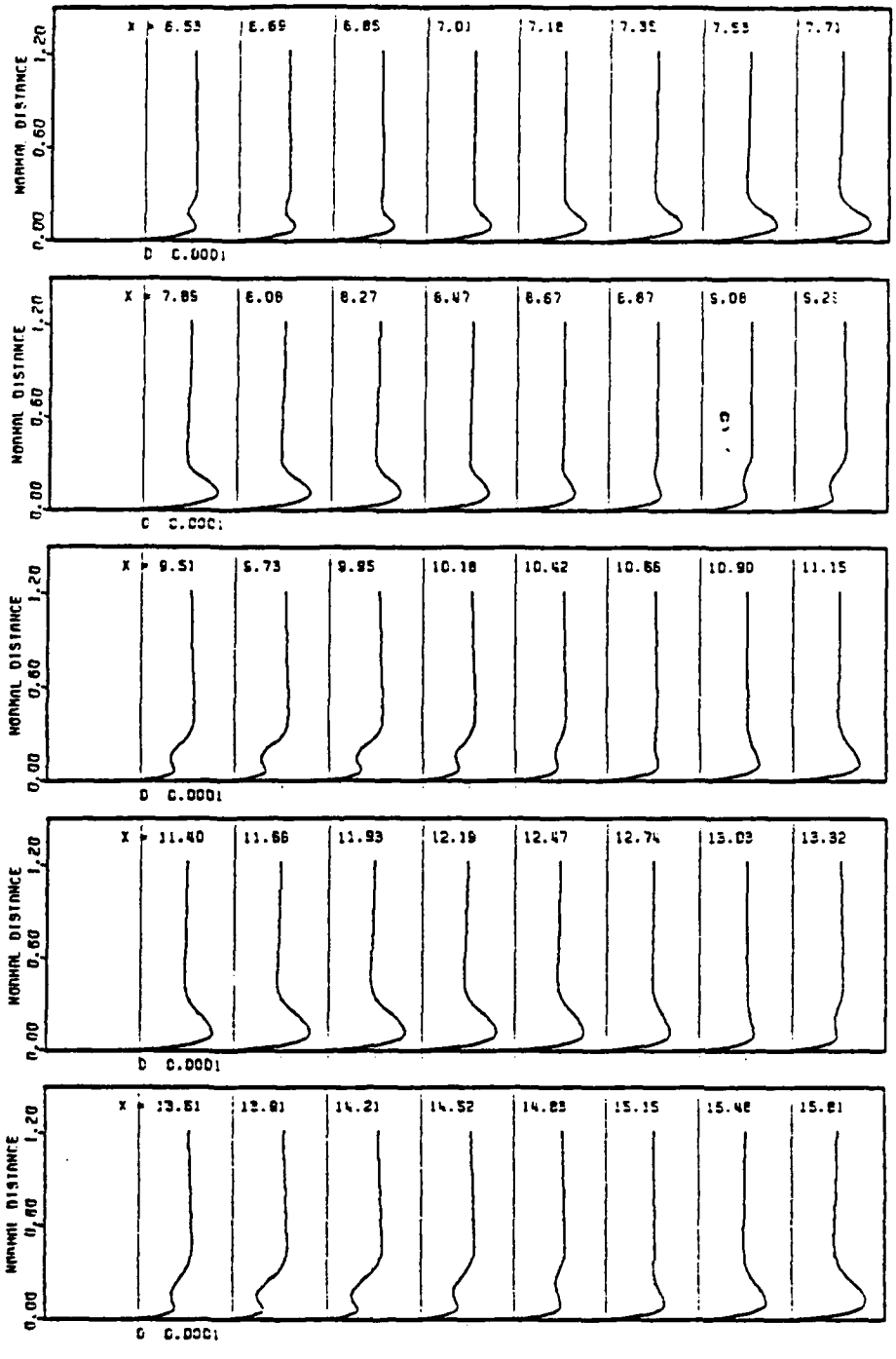

Figure 19a. Continued.

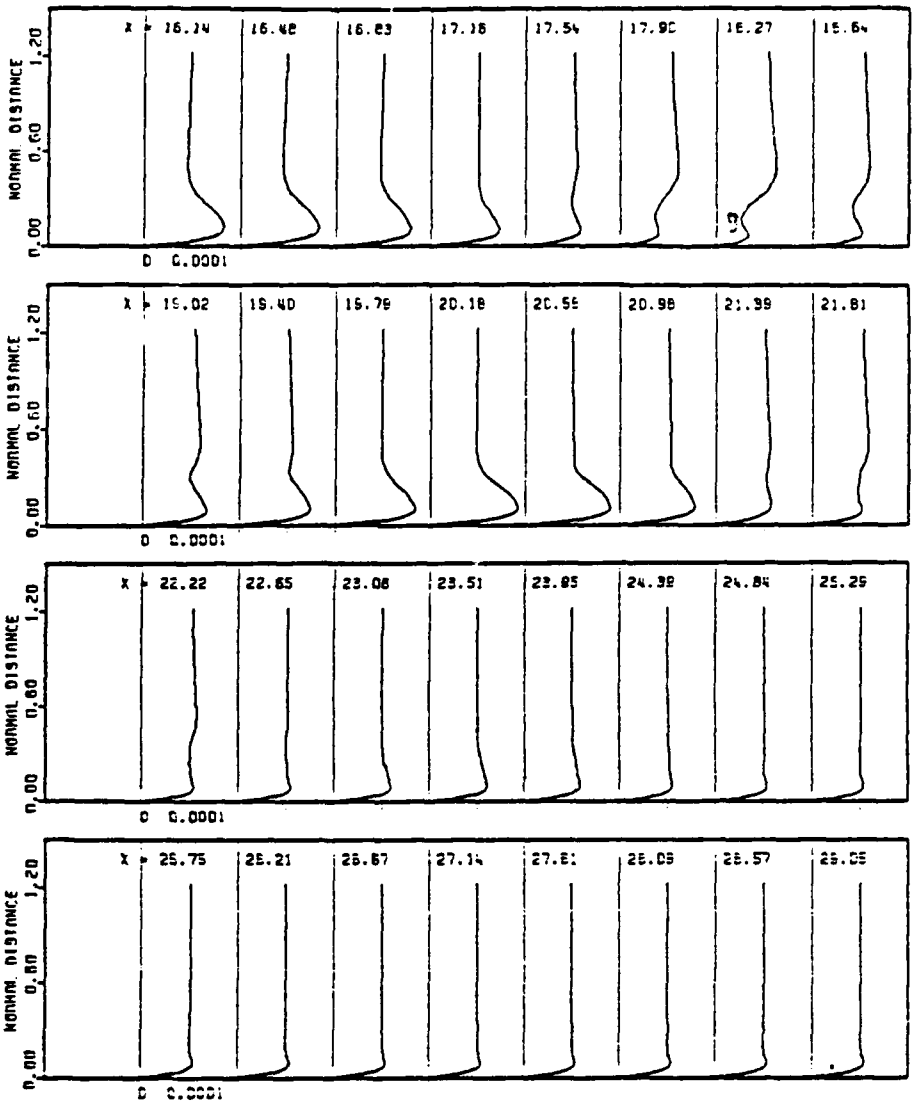

Figure 19a. Continued.

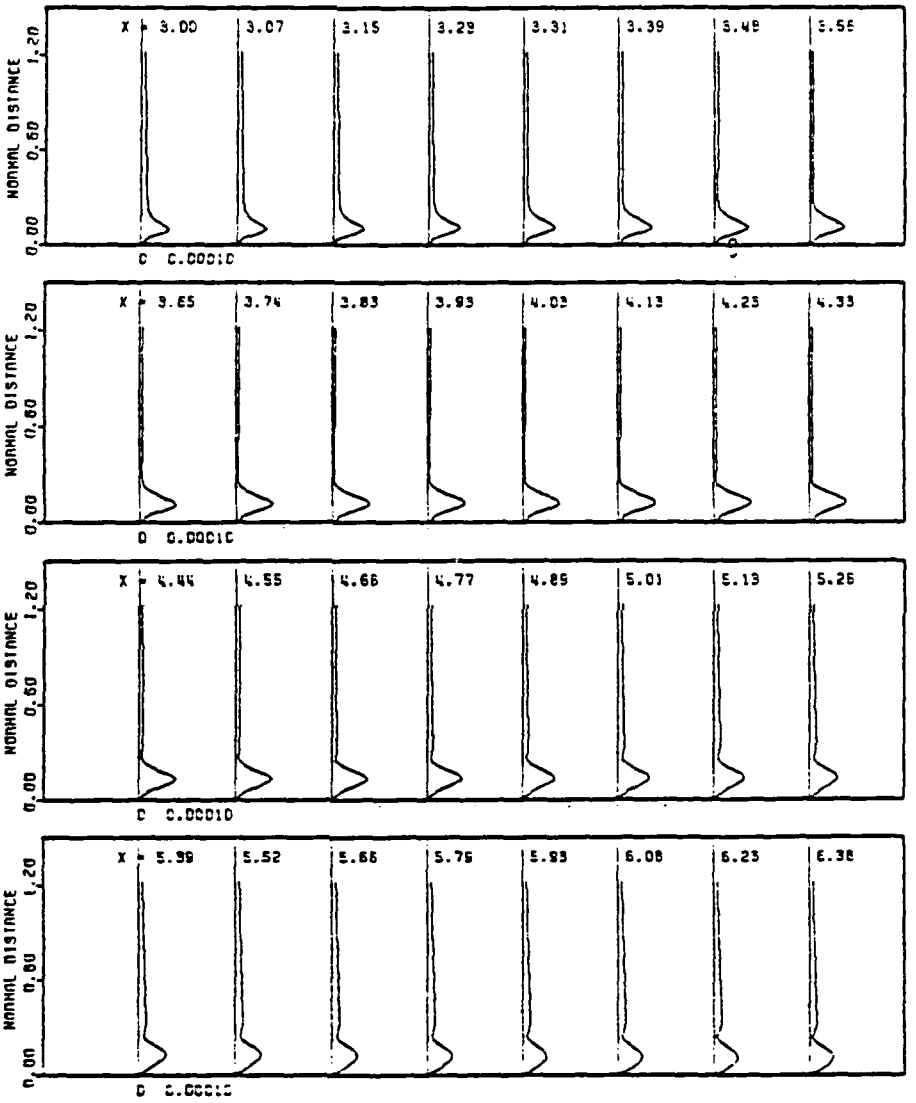

Figure 20. Amplitude profiles of streamwise perturbation velocity u' taken during the fifth cycle at consecutive downstream locations after the Stokes wave is subtracted; $F = 230$, $a_S = 0.0001$.

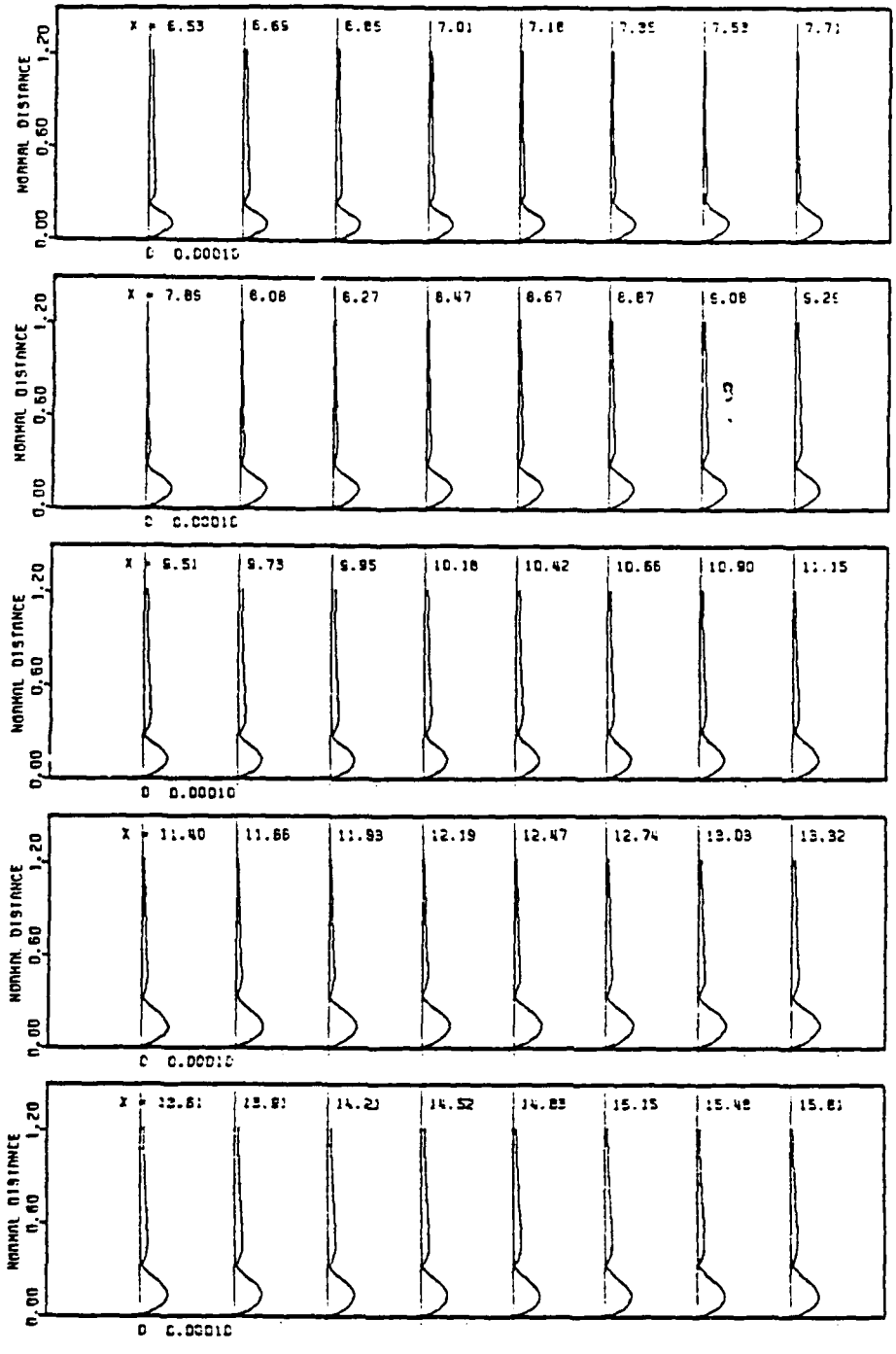

Figure 20a. Continued.

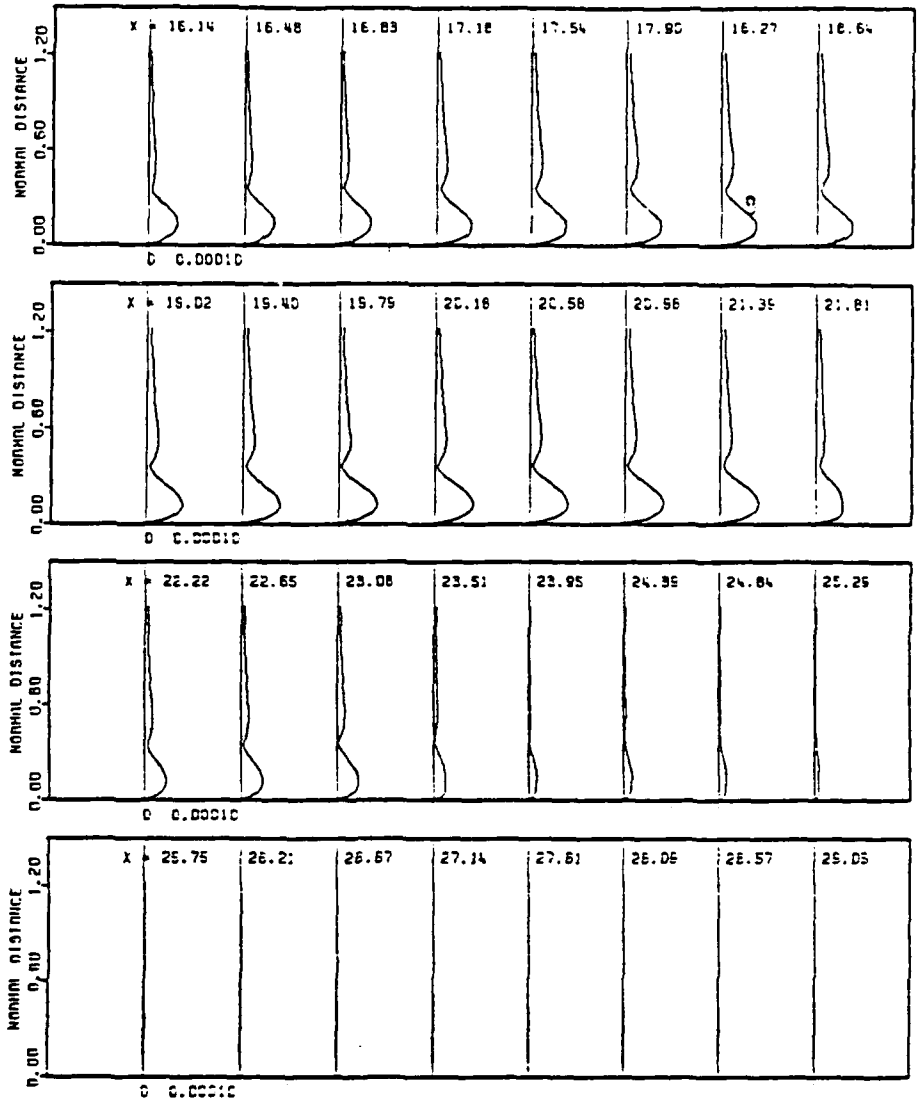

Figure 20a.Continued.